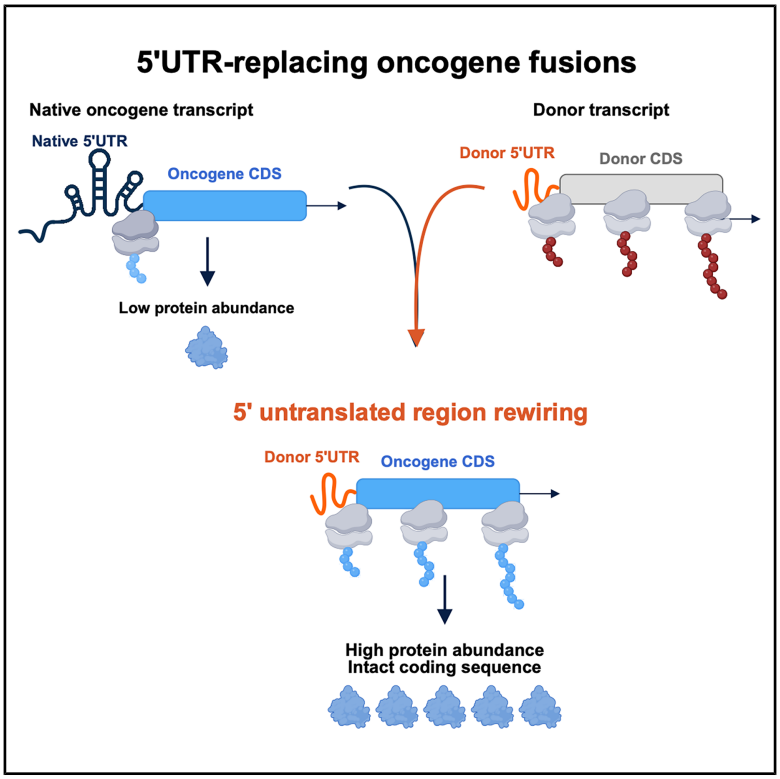
Cell Reports

Article

Untranslated region rewiring defines a novel class of oncogene fusions

Graphical abstract



Highlights

- 5′ UTR-replacing fusions define a new class of oncogene fusions
- Donor-derived 5′ UTRs rewire oncogene translational control
- 5′ UTR rewiring increases oncogene expression without altering protein sequence
- This mechanism extends beyond MET to multiple oncogenes

Authors

Marina Cerqua, Estelle Bigot, Cédric Chaveroux, Paolo M. Comoglio, Dogus M. Altintas

Correspondence

pcomoglio@gmail.com (P.M.C.), dogus.altintas@gmail.com (D.M.A.)

In brief

Cerqua et al. identify a previously unrecognized class of oncogene fusions in which native oncogene 5′ untranslated regions (5′ UTRs) are replaced by donor-derived 5′ UTRs. This rewiring of translational control increases expression from intact protein-coding sequences and extends across multiple oncogenes.

Cerqua et al., 2026, Cell Reports *45*, 118145
October 27, 2026 © 2026 The Author(s). Published by Elsevier Inc.
https://doi.org/10.1016/j.celrep.2026.118145

CellPress

Cell Reports

CellPress
OPEN ACCESS

Article

Untranslated region rewiring defines a novel class of oncogene fusions

Marina Cerqua,[1] Estelle Bigot,[2] Cédric Chaveroux,[2] Paolo M. Comoglio,[1,4,*] and Dogus M. Altintas[1,2,3,4,5,*]
[1]IFOM ETS-The AIRC Institute of Molecular Oncology, 20139 Milano, Italy
[2]Laboratoire de Biologie Tissulaire et Ingénierie Thérapeutique (LBTI), UMR CNRS 5305, Institut de Biologie et Chimie des Protéines, Université Claude Bernard Lyon 1, Lyon, France
[3]Senior author
[4]These authors contributed equally
[5]Lead contact
*Correspondence: pcomoglio@gmail.com (P.M.C.), dogus.altintas@gmail.com (D.M.A.)
https://doi.org/10.1016/j.celrep.2026.118145

SUMMARY

Gene fusions in cancer are traditionally understood to generate hybrid proteins with altered functions that promote malignancy. Here, we define a previously unrecognized class of oncogenic fusions that preserve protein structure but replace the 5′ untranslated region (5′ UTR), thereby rewiring translational regulation. Using the *MET* oncogene as a paradigm, we show that 5′ UTR-replacing fusions, identified across >200,000 cancer samples, increase MET protein abundance 5- to 10-fold without corresponding changes in mRNA levels. The resulting receptor remains correctly localized, ligand-responsive, and active, thereby promoting cell survival and motility. These fusion transcripts are detected following irradiation, documenting UTR rewiring in a post-treatment context. Beyond *MET*, similar 5′ UTR-replacing fusions occur in *FGFR1*, *JAK2*, and *NTRK2*, where partner-derived 5 ′UTRs are associated with reduced regulatory complexity and enhanced protein output. Together, our findings establish UTR rewiring as an overlooked mechanism of oncogene overexpression with implications for cancer genome annotation and precision oncology.

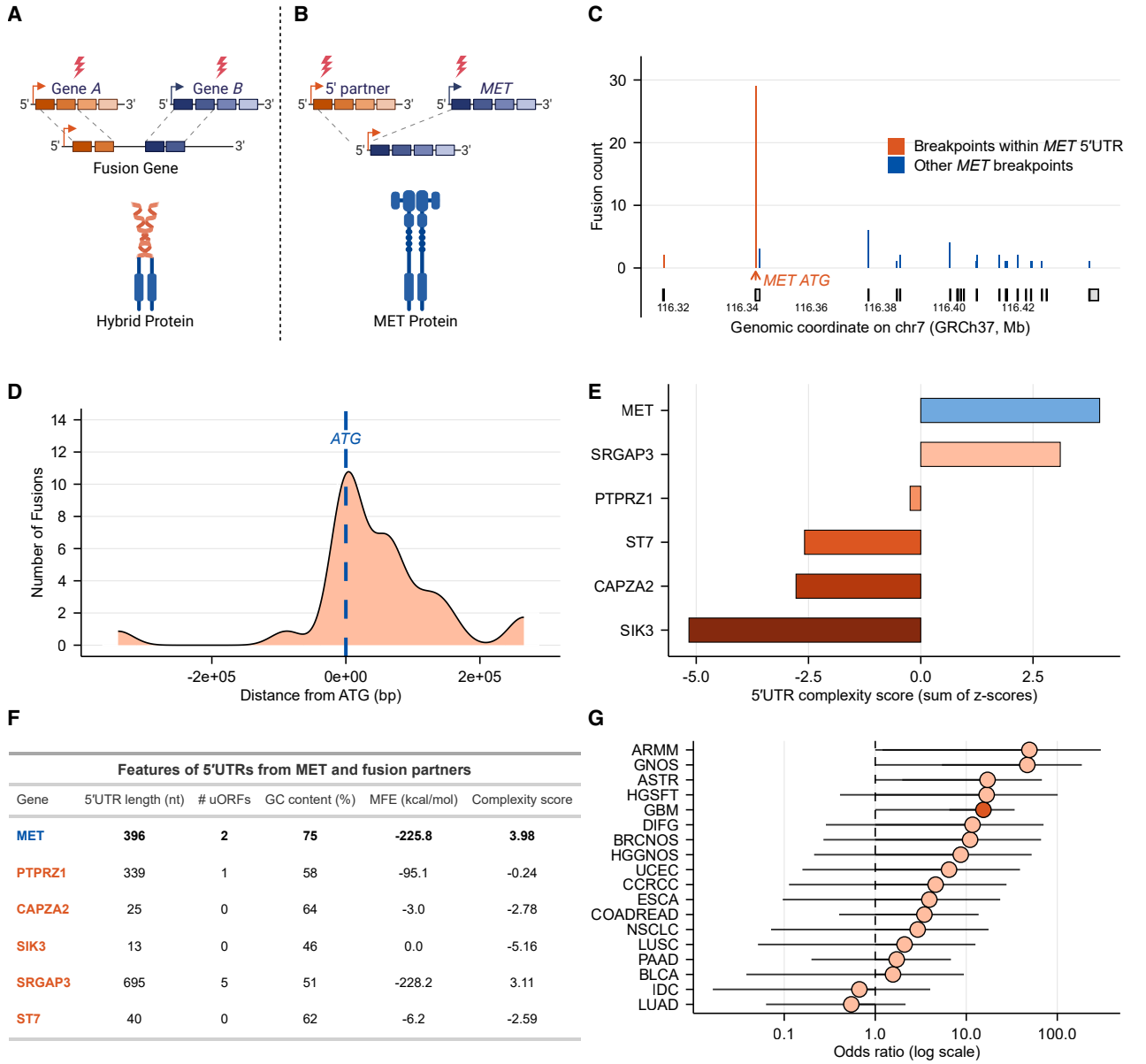
INTRODUCTION

Fusion genes are a hallmark of cancer and are classically understood to drive malignancy through the generation of hybrid proteins with altered structure and function.[1–5] These chimeric proteins often combine regulatory and catalytic domains from donor genes, resulting in constitutive activation, loss of regulation, or neomorphic properties.[6–8] Canonical examples include the *BCR-ABL* fusion[9,10] in chronic myeloid leukemia and various *RET* fusions in thyroid and lung cancers,[11,12] *ALK* fusions in lung adenocarcinoma and non-Hodgkin lymphoma[13,14] and *MET* fusions reported in lung adenocarcinoma and glioblastoma,[15,16] all of which activate kinase signaling in an uncontrolled manner. MET, the receptor for hepatocyte growth factor (HGF), promotes cell motility, growth, and survival, and is frequently implicated in tumor progression across cancer types.[17–20] Well-characterized experimental models such as *TPR-MET*, together with clinically observed fusions including *KIF5B-MET*, yield structurally modified receptors with heightened kinase activity and transforming potential.[15,16,21–23]

While analyzing large-scale cancer genomics datasets (AACR GENIE v17.0 dataset[24]), we made the unexpected observation that a subset of *MET* fusion calls indicate junction positions immediately upstream of the start codon (ATG), preserving the entire open reading frame. These fusion events replace the native (i.e., wild-type [WT]) 5′ untranslated region (5′ UTR) with regulatory elements from unrelated genes—a previously underappreciated fusion architecture that implicates a non-coding mechanism of translational deregulation. The 5′ UTR is a critical regulatory element that modulates translation efficiency through multiple cis-regulatory features, including RNA secondary structure, (guanine-cytosine (GC) content, and upstream open reading frames (uORFs).[25–28] Although translational control via 5′ UTRs is well established,[25] whether gene fusions can rewire UTRs to modulate oncogene expression has not been systematically examined.[8] In our previous study, we demonstrated that the native 5′ UTR of *MET* is unusually complex and acts as a translational brake, limiting protein output independently of mRNA levels.[29]

Prompted by this structural pattern and our prior insights into *MET* translational control, we investigated the impact of 5′ UTR-replacing fusions on MET protein expression and function. Here, we show that such events lead to a 5- to 10-fold increase in protein expression without affecting mRNA abundance. The resulting receptor is identical in size to the WT protein and properly membrane-localized, but exhibits heightened expression, leading to increased ligand responsiveness in fusion-harboring cells. Replacement of the *MET* 5′ UTR fosters hallmark oncogenic behaviors, including motility and survival. Following irradiation, 5′ UTR-replacing *MET* fusion transcripts were detected in cells isolated from a parental WT population,

This is an open access article under the CC BY license (http://creativecommons.org/licenses/by/4.0/).



Features of 5′UTRs from MET and fusion partners

Gene	5′UTR length (nt)	# uORFs	GC content (%)	MFE (kcal/mol)	Complexity score
MET	**396**	**2**	**75**	**-225.8**	**3.98**
PTPRZ1	339	1	58	-95.1	-0.24
CAPZA2	25	0	64	-3.0	-2.78
SIK3	13	0	46	0.0	-5.16
SRGAP3	695	5	51	-228.2	3.11
ST7	40	0	62	-6.2	-2.59

Figure 1. *MET* fusion junction positions cluster near the translation start site

(A) Canonical fusion mechanism: chromosomal rearrangements join the coding sequences of two genes to create a hybrid protein with altered structure and function. Shown is the example of TPR-MET, in which the coiled-coil domain of TPR (orange) is fused to the kinase domain of MET (blue).

(B) In a distinct subset of fusion events, this fusion occurs upstream of the MET start codon, replacing the native 5′ UTR while preserving the entire coding sequence and yielding a wild-type MET protein.

(C) Distribution of retained *MET*-side fusion junction position in human cancers (AACR Project GENIE v17.0-public). After filtering, 182 MET fusion calls with precisely annotated *MET*-side junction positions were retained for analysis (Table S1). Of these, 37 (20.3%) occurred upstream of the canonical MET translation start site (ATG), including 34 (18.7%) within the annotated MET 5′ UTR. Junction positions within the annotated *MET* 5′ UTR are shown in orange; all other retained sequences are shown in blue.

(D) Junction positions in donor genes are similarly enriched upstream of their respective ATGs, indicating selective replacement of 5′ regulatory regions rather than coding sequences. The density plot shows fusion counts relative to the donor gene start codon (canonical transcript).

(E) Comparison of composite 5′ UTR complexity scores for MET and representative donor genes involved in MET fusions. MET displays a markedly higher composite 5′ UTR complexity score, whereas the corresponding reference donor 5′ UTRs show lower complexity values. The composite complexity score integrates z scored 5′ UTR length, upstream open reading frame (uORF) count, GC content, and normalized RNA secondary-structure stability (−minimum free energy (MFE) per nucleotide), as described in STAR Methods.

(legend continued on next page)

documenting UTR rewiring in a post-treatment context. Beyond *MET*, we identify similar 5′ UTR-replacing fusions in other oncogenes, including *FGFR1*, *JAK2*, and *NTRK2*, with donor 5′ UTRs displaying simplified, translation-permissive features.

These findings define a previously unrecognized class of gene fusions that enhance oncogene expression through "UTR rewiring": a non-coding mechanism that increases protein output and expands the functional impact of gene rearrangements in cancer biology.

RESULTS

A significant proportion of MET fusion junction positions cluster near the translation start site

To examine the architecture of *MET* fusions in human tumors, we analyzed large-scale genomic data from the AACR Project GENIE (v17.0), encompassing over 229,000 sequenced samples from more than 196,000 patients.[24] Unexpectedly, a notable fraction of *MET* fusion calls contained transcript junctions immediately upstream of the annotated start codon (GenBank: NM_000245.4), preserving the complete open reading frame. Rather than altering the coding sequence, these fusion calls were consistent with replacement of the native *MET* 5′ UTR by sequences mapping to annotated non-coding regions of unrelated genes (Figures 1A and 1B). This fusion-junction distribution contrasted with canonical kinase-activating fusions that generate structurally modified proteins, suggesting instead a potential non-coding mechanism of oncogene regulation.

To rigorously characterize these events, we restricted our analysis to *MET* fusion calls with precisely annotated junction positions relative to the canonical *MET* ATG, following a stringent multi-step filtering strategy (Table S1). This analysis identified 182 *MET* fusion calls with well-resolved *MET*-side junctions, among which 34 (18.7%) occurred within the annotated *MET* 5′ UTR upstream of the canonical ATG, thereby preserving the entire open reading frame (Figure 1C; Table S2). Sensitivity analyses using alternative junction position windows relative to the ATG produced consistent enrichment patterns (Table S3). Most retained *MET* fusion calls in GENIE are supported by RNA sequencing-based evidence (Table S4). Independent analyses of The Cancer Genome Atlas (TCGA) fusion datasets using the same junction position classification framework further corroborated the presence of *MET* fusions preserving the full coding sequence (Table S5).

Strikingly, junction positions in the donor genes were similarly concentrated in proximity to their respective start codons, consistent with a selective replacement of regulatory rather than coding sequences (Figure 1D). Despite the functional diversity of the donor genes (Table S2), the corresponding reference 5′ UTRs shared a defining feature: they were structurally simpler than the native *MET* 5′ UTR. The 5′ UTR is a key determinant of translation efficiency, shaped by several cis-regulatory features such as GC-rich sequences that promote stable RNA secondary structures that hinder ribosome scanning, and uORFs, which can divert ribosomes from the main start codon.[30,31] To quantify RNA folding propensity, we used minimum free energy (MFE) calculations—a computational measure of how tightly the 5′ UTR folds on itself.[32] The native *MET* 5′ UTR is notably complex: it spans 396 nucleotides, contains two uORFs, has a high GC content of 75%, and forms stable secondary structures with an MFE of −225.8 kcal/mol (Figures 1E and 1F). To summarize these mechanistically relevant features into a single descriptive metric, we defined a composite 5′ UTR complexity score (length, uORFs, GC content, and normalized folding stability), intended to integrate multiple regulatory features associated with translational efficiency. Consistent with this interpretation, partner-derived sequences corresponding to annotated 5′ UTRs generally display lower composite complexity scores than the native *MET* 5′ UTR (Figures 1E and 1F). These fusion architectures were observed across multiple cancer types, with significant enrichment in glioblastoma (Figure 1G; Table S6).

These observations suggest that fusion-mediated replacement of the native 5′ UTR relieves key translational constraints and is associated with enhanced MET protein output, not by altering the protein sequence, but by rewiring its 5′ UTR-dependent translational regulation.

Partner-derived 5′ UTRs increase MET protein output

To test whether this translational rewiring affects translation, we used a dual-luciferase reporter assay in which each 5′ UTR was cloned upstream of a NanoLuc reporter and co-transfected with a firefly luciferase control. The native *MET* 5′ UTR significantly suppressed NanoLuc activity by more than 10-fold as compared to the empty vector lacking a 5′ UTR (No 5′ UTR control, i.e., containing only a Kozak sequence to permit efficient translation initiation). In contrast, all partner-derived 5′ UTRs resulted in markedly higher NanoLuc expression, sometimes exceeding a 25-fold increase compared to the native *MET* 5′ UTR despite comparable mRNA levels (Figures 2A and 2B; Figures S1A and S1B). These findings indicate that donor 5′ UTRs replacing the native *MET* 5′ UTR can lift the translational blockade.

To assess whether the observed increase in translational efficiency was enough to raise MET protein levels, we transfected expression vectors containing the entire *MET* coding sequence under the same promoter, differing only in their 5′ UTR composition (either the native *MET* 5′ UTR, no UTR, *CAPZA2* 5′ UTR, or *ST7* 5′ UTR). Western blotting showed that replacement of the native 5′ UTR with partner-derived 5′ UTRs significantly increased MET protein expression without a corresponding change in MET mRNA levels (Figure 2C). This increase was accompanied by higher absolute levels of phosphorylated MET (p-MET) and downstream signaling (Figure S1C).

To directly assess the contribution of 5′ UTR replacement independently of genomic rearrangements or promoter alterations,

(F) Individual features contributing to 5′ UTR complexity for MET and selected fusion partners, including 5′ UTR length, number of uORFs, GC content, MFE, and composite complexity score. MFE values were computed using ViennaRNA v2.7.2.

(G) Enrichment of MET 5′ UTR-replacing fusions across cancer types (within the subset of fusions with precisely annotated junction positions). Odds ratios (log scale) were computed using Fisher's exact test. Error bars denote 95% confidence intervals. Red intensity indicates tumor type with significant enrichment after multiple-testing correction (Benjamini-Hochberg, adjusted $p < 0.05$). Tumor codes in the *y* axis are listed in Table S6.

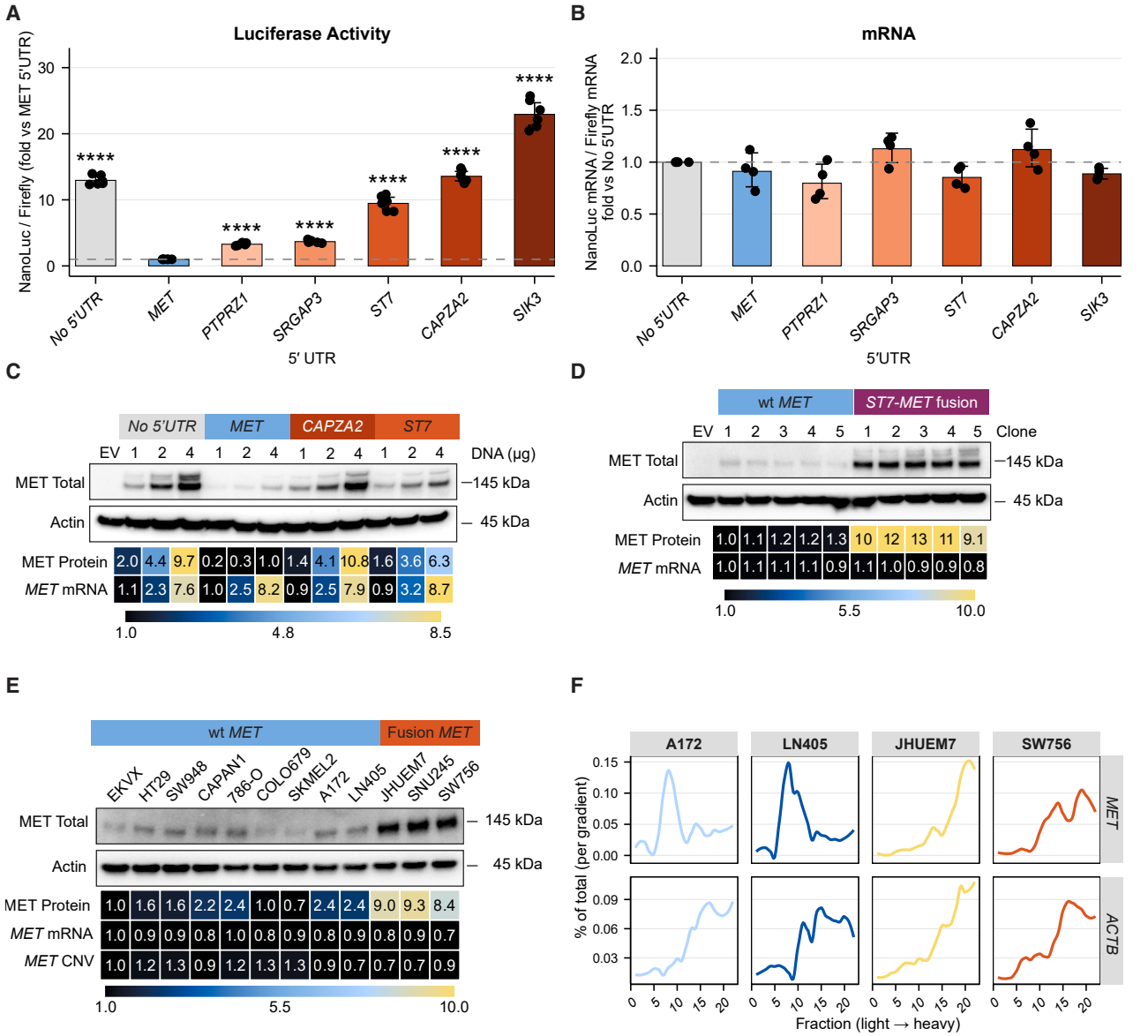


Figure 2. Partner-derived 5′ UTRs promote MET overexpression through enhanced translation

(A) Luciferase reporter assay measuring translation of native or partner-derived 5′ UTRs. Each 5′ UTR was cloned upstream of NanoLuc luciferase and co-transfected with a firefly luciferase vector for internal normalization. Data represent mean ± SEM from $n = 6$ independent biological replicates. Statistics were performed on NanoLuc/firefly ratios using one-way ANOVA followed by Dunnett's post hoc test versus the native MET 5′ UTR. ****$p < 0.0001$.

(B) Relative NanoLuc mRNA levels measured by reverse transcription-quantitative polymerase chain reaction (RT-qPCR) from the same transfections as in (A), normalized to firefly mRNA. Ratios are expressed relative to no 5′ UTR (mean ± SEM, $n = 4$). No significant differences were observed (one-way ANOVA with Dunnett's post hoc test; adjusted $p > 0.05$).

(C) Western blot analysis of MET protein output from expression vectors containing either no 5′ UTR, the native *MET* 5′ UTR, or partner-derived 5′ UTRs (*CAPZA2* or *ST7*), transfected into MET-negative TOV112D cells. For MET, the upper (~175 kDa) and lower (~145 kDa) bands correspond to the precursor and mature forms of MET, respectively. Actin was used as a loading control. Quantification was performed on the mature MET band normalized to actin ($n = 3$ independent experiments). *MET* mRNA levels were measured by RT-qPCR from matched samples and normalized to *TBP*.

(D) T47D cells expressing *MET* with either native or partner-derived (*ST7*) 5′ UTRs. Western blot and RT-qPCR analyses show increased MET protein levels despite comparable *MET* mRNA abundance. Five independent clones per condition were analyzed.

(E) MET protein expression in fusion-positive (orange) and fusion-negative (blue) cancer cell lines from Cancer Cell Line Encyclopedia (CCLE). Immunoblots show total MET and actin. Heatmaps display quantified MET protein, relative *MET* mRNA (ΔΔCt, *TBP* reference), and *MET* copy number (CNV, ΔΔCt, *hTERT* reference). Data were obtained from $n = 3$ independent biological replicates per cell line.

(F) Polysome profiling analysis of mRNA distribution across ribosomal fractions. Differences in ribosome occupancy were analyzed by mixed-effects two-way ANOVA (gene × cell line) with Kenward-Roger approximation and Holm-adjusted post hoc contrasts (representative curves shown; $n = 3$ biological replicates per cell line). In fusion-positive cell lines (JHUEM7 and SW756), *MET* mRNA is significantly shifted toward heavier gradient fractions, displaying an actin-like distribution ($p < 0.0001$).

we established matched T47D cell lines expressing *MET* constructs that differ exclusively in their 5′ UTR sequences (native versus ST7-derived), while retaining identical coding regions and promoter contexts. This experimental design isolates the effect of UTR rewiring on protein output while avoiding additional variables associated with endogenous genome engineering. In this controlled genetic background, replacement of the native *MET* 5′ UTR significantly increased MET protein expression despite comparable *MET* mRNA levels (Figure 2D). These findings demonstrate that replacement of the native 5′ UTR is sufficient to increase MET protein output.

To determine whether these observations extended to endogenous 5′ UTR-replacing *MET* fusions, we examined the Cancer Cell Line Encyclopedia[33] and DepMap[34] datasets. We identified three *MET* fusion-positive cell lines: JHUEM7 (endometrial cancer, CAPZA2-MET fusion), SNU245 (extrahepatic cholangiocarcinoma, *ST7-MET* fusion), and SW756 (cervical squamous cell carcinoma, *ST7-MET* fusion). Sanger sequencing confirmed the precise fusion junction positions and demonstrated that the entire *MET* coding sequence was preserved in frame, with no additional coding mutations (Figures S2 and S3A).

Consistent with the observations in the matched T47D model, *MET* fusion-positive cell lines displayed increased MET protein levels despite comparable *MET* mRNA expression and *MET* gene copy number relative to nine MET WT cell lines from various tissues of origin (Table S7; Figure 2E). Western blots showed the expected precursor (~175 kDa) and mature (~145 kDa) forms of MET, with no additional higher or lowermolecular-weight species detected, confirming that these rearrangements do not generate hybrid MET proteins.

To determine whether increased MET protein levels reflected enhanced translation rather than altered protein stability, we first assessed MET protein turnover using cycloheximide chase assays. MET half-life was comparable between WT and fusion conditions (Figures S3B and S3C), indicating that the increase was not explained by altered degradation. We then performed polysome profiling, which revealed increased association of *MET* fusion transcripts harboring partner-derived 5′ UTRs with heavy polysome fractions (Figure 2F; Figure S3D), consistent with enhanced translational efficiency.

MET expressed from 5′ UTR-replacing fusions is properly localized and ligand-dependent

Having shown that 5′ UTR-replacing fusions elevate MET protein levels without altering mRNA abundance or coding sequence, we next assessed whether the resulting MET receptor is correctly localized and functionally competent. MET is a receptor tyrosine kinase that resides at the plasma membrane and becomes activated upon binding to HGF, a paracrine ligand secreted by mesenchymal cells.[17,35–37] HGF binding induces receptor dimerization, autophosphorylation, and internalization, triggering downstream signaling pathways that promote cell migration and survival (i.e., invasive growth).[18,38,39]

To evaluate ligand responsiveness, we stimulated fusion-positive or WT cell lines with increasing concentrations of HGF (0–100 ng/mL) and monitored MET phosphorylation by western blot. MET phosphorylation was detectable at 10 ng/mL HGF in fusion-positive cell lines (JHUEM7, SNU245, and SW756). In contrast, WT lines (A172 and LN405) required high doses (Figure 3A). This suggests that elevated receptor levels in fusion-positive cells confer increased responsiveness to ligand stimulation. We then examined receptor localization. As shown by immunofluorescence (Figure 3B; Figure S4A) and flow cytometry (Figure 3C), MET is properly localized at the cell surface. Upon HGF exposure, both WT and fusion-positive cells exhibited a time-dependent reduction in surface MET levels, consistent with the expected ligand-induced receptor internalization (Figure 3D).[36,40] These results demonstrate that *MET* expressed from 5 ′UTR-replacing fusions is correctly localized and functionally regulated, behaving like the WT receptor but expressed at higher levels. These findings were independently validated in T47D cells stably expressing the *ST7-MET* fusion, which exhibited enhanced HGF-induced MET phosphorylation compared to WT controls (Figure 3E). This phosphorylation was inhibited by tepotinib, a selective, FDA-approved MET inhibitor.[41] Immunofluorescence analyses further confirmed membrane localization of MET in both WT and *ST7-MET*-expressing T47D cells, as evidenced by co-localization with the cell surface marker E-cadherin (Figure 3F).

Unlike previously described oncogenic *MET* fusions that yield structurally modified, constitutively active receptors (e.g., *TPR-MET*,[15,42] *KIF5B-MET*[22]), these rearrangements do not alter MET's architecture or activation mechanism.

MET expressed from 5′ UTR-replacing fusion transcripts is functional

MET signaling is known to support cell survival and migration, especially under stress conditions such as radiotherapy or tissue damage.[17,29,39,43–46] 5′ UTR fusion-positive cell lines (JHUEM7, SNU245, and SW756) and WT counterparts (A172 and LN405) were subjected to irradiation followed by increasing concentrations of HGF. All lines exhibited a dose-dependent short-term (Figures 4A–4C; Figures S4B and S4C) and long-term (Figures 4D–4F; Figures S4D–S4F) survival. Tepotinib prevented this radio-protective effect. Furthermore, SW756 5′ UTR fusion-positive cells responded to HGF with a scattering phenotype—characterized by the dissociation of compact epithelial colonies into dispersed, spindle-like cells—a hallmark morphological response of HGF/MET signaling.[47,48] This effect was suppressed by tepotinib (Figure S4G). Consistently, wound healing assays demonstrated HGF-dependent wound closure, a response also abrogated by tepotinib (Figures S4H–S4J).

To assess whether 5′ UTR rewiring-induced MET overexpression confers a functional advantage within a matched genetic background, we compared T47D cells stably expressing either WT or *ST7-MET* fusion. Following irradiation, HGF increased short-term survival. The response was consistently greater in *ST7-MET* fusion cells relative to WT controls (Figures 4G and 4H). This enhancement was corroborated in clonogenic assays, where *ST7-MET* fusion cells formed more colonies after genotoxic stress (Figures S5A–S5C). Beyond survival, *ST7-MET* fusion potentiated HGF-driven phenotypic changes, including stronger induction of the mesenchymal marker alpha-smooth muscle actin (α-SMA),

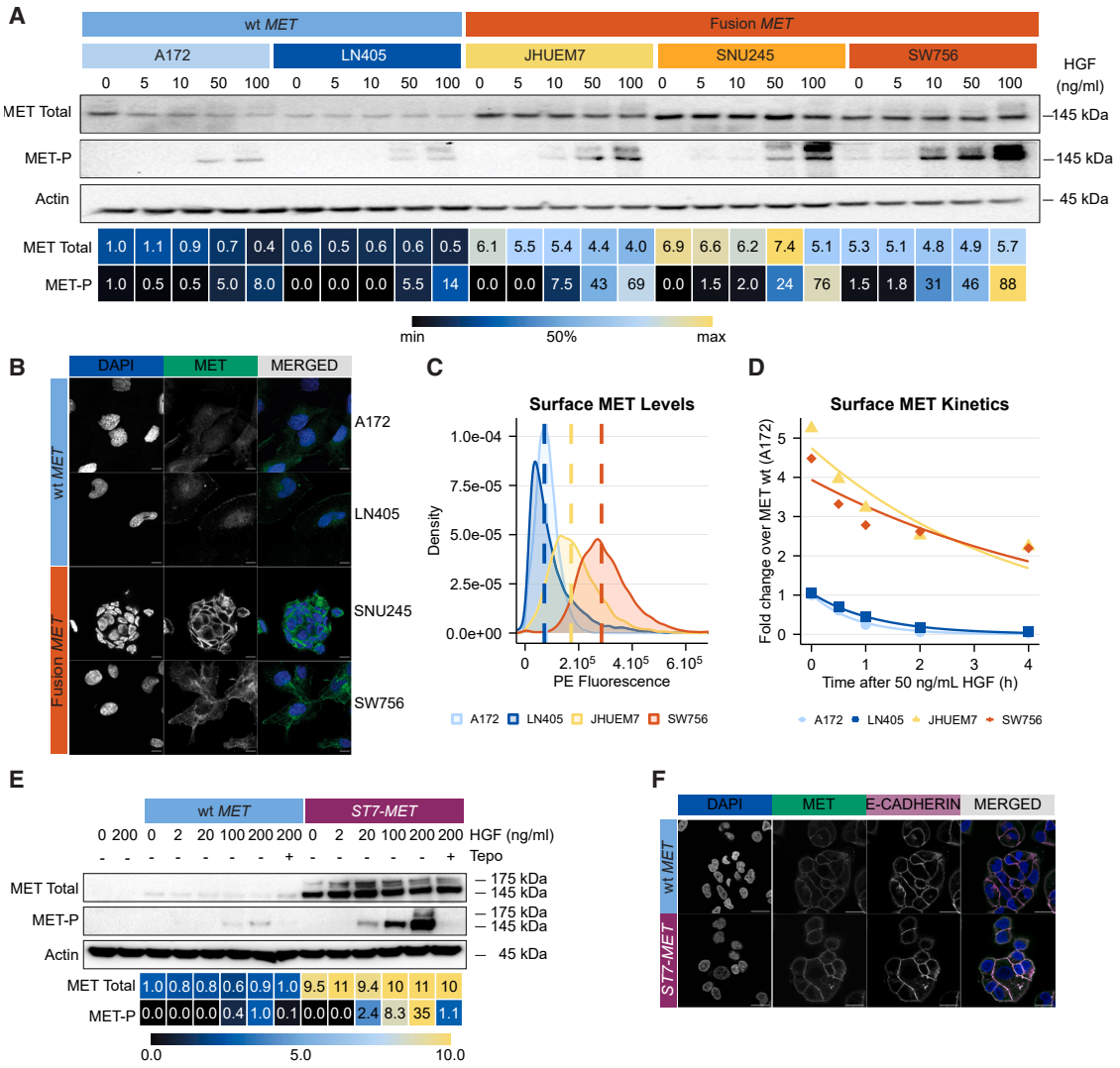


Figure 3. MET expressed from 5′ UTR-replacing fusions retains proper membrane localization and ligand-dependent activation

(A) Western blot analysis of total MET and MET phosphorylation (Y1234/1235) in wild-type (A172 and LN405) or fusion-positive (JHUEM7, SNU245, and SW756) cell lines after 15 min stimulation with increasing concentrations of HGF. Representative blots from $n = 3$ independent biological experiments are shown.

(B) Representative confocal microscopy images ($n = 3$ independent experiments) showing surface MET (green) localization in wild-type (top) and fusion-positive (bottom) cell lines. Nuclei stained with 4';6-diamidino-2-phenylindole (DAPI, blue). Scale bars, 25 μm.

(C) Flow cytometry density plots of surface MET levels (phycoerythrin, PE fluorescence) in wild-type (A172 and LN405) and fusion-positive (JHUEM7 and SW756) cell lines. Dashed lines mark median values.

(D) Representative flow cytometry analysis assessing surface MET exposure following treatment with 50 ng/mL HGF in wild-type (A172 and LN405) and fusion-positive (JHUEM7 and SW756) cell lines. Values are shown as fold change over baseline A172.

(E) Western blot analysis of MET phosphorylation in T47D cells stably expressing wild-type *MET* or *ST7-MET* following 15 min stimulation with increasing concentrations of HGF. Blots are representative of $n = 3$ independent biological experiments.

(F) Confocal immunofluorescence showing co-localization of MET with E-cadherin in T47D cells expressing either wild-type *MET* or *ST7-MET* fusion. Scale bars, 25 μm ($n = 3$ independent experiments). For flow cytometry experiments, the gating strategies are shown in Data S2.

consistent with epithelial-to-mesenchymal transition (EMT)-associated features (Figures S5D and S5E). Wound healing assays demonstrated increased HGF-dependent wound closure in *ST7-MET* fusion cells compared with WT counterparts (Figures 4I–4K). Together, these data indicate that 5′ UTR-mediated MET overexpression enhances the magnitude of canonical ligand-dependent signaling outputs.

5′ UTR-replacing MET fusion transcripts are detected following irradiation

Having established that 5′ UTR replacement enhances *MET* translational output and preserves receptor functionality, we next asked whether 5′ UTR-replacing fusion transcripts could be detected under defined genotoxic stress conditions. To address this, we used A172 glioblastoma cells, which

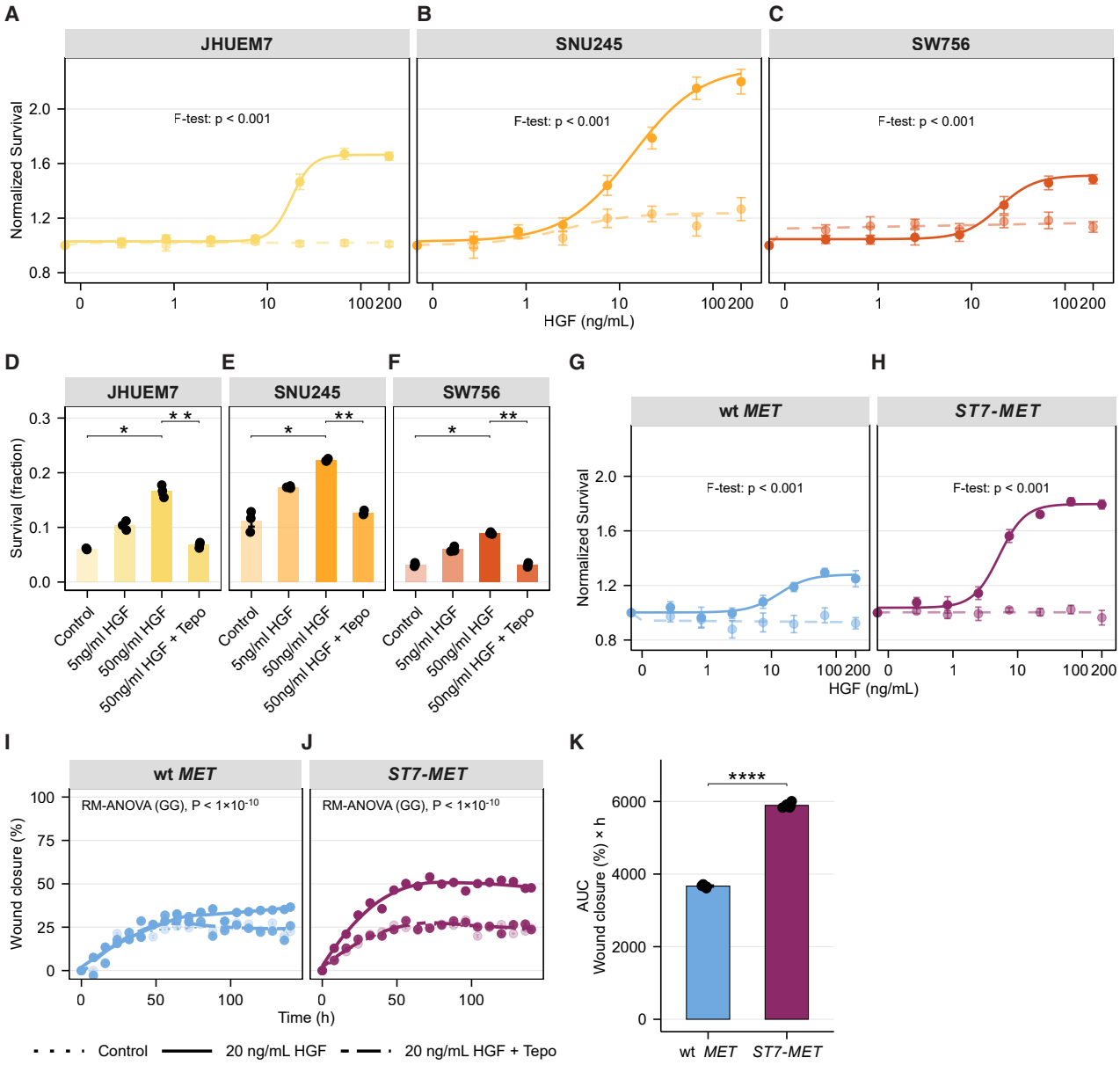


Figure 4. MET expressed from 5′ UTR-replacing fusion transcripts is functional

(A–C) Survival of JHUEM7 (A), SNU245 (B), and SW756 (C) fusion-positive cell lines 48 h post-irradiation (7.5 Gy). HGF promotes a dose-dependent increase in survival, which is suppressed by the MET inhibitor tepotinib (50 nM, dashed lines). Data shown as mean ± SEM, $n = 6$ biological replicates. Dose-response curves were fitted by nonlinear regression; differences between curves were assessed using the extra sum-of-squares F-test.

(D–F) Clonogenic survival assays of irradiated fusion-positive JHUEM7 (D), SNU245 (E), and SW756 (F) cells treated with indicated concentrations of HGF ± tepotinib (50 nM). Colonies were fixed and stained with crystal violet after 10–14 days. Data represent mean ± SEM from $n = 3$ independent biological replicates, each performed in technical duplicate. Individual biological replicates are shown as dots. Statistical analysis was performed using one-way ANOVA with Tukey's multiple-comparisons test (*$p < 0.05$; **$p < 0.01$).

(G and H) Dose-response survival curves in T47D cells expressing either wild-type *MET* (G) or *ST7-MET* fusion (H) ± tepotinib (50 nM, dashed lines). *ST7-MET* fusion confers enhanced HGF responsiveness compared to wild-type controls. Data represent mean ± SEM, $n = 6$ independent biological replicates. Significance assessed by nonlinear regression comparison (extra sum-of-squares F-test).

(I and J) Wound-healing assays of T47D expressing wild-type *MET* (I) or *ST7-MET* fusion (J) cells treated with HGF ± tepotinib (50 nM, dashed lines). Data represent mean ± SEM, $n = 6$ independent biological replicates. Statistical significance was determined using repeated-measures ANOVA with Greenhouse-Geisser correction.

(K) Area under the curve (AUC) of wound closure over time (0–140 h) for T47D wild-type and *ST7-MET* fusion cells under HGF stimulation (20 ng/mL). AUC was calculated for each independent biological replicate ($n = 6$) using the trapezoidal method. Bars represent mean ± SEM; dots represent individual replicates. Statistical significance was determined by unpaired two-tailed *t* test (****$p < 0.0001$).

predominantly express WT MET with its native 5′ UTR. We first confirmed that this model mounts an effective DNA damage response following irradiation. The DNA damage marker, γH2AX, was rapidly induced within 30 min after 7.5 Gy exposure and progressively declined over 48 h, consistent with active DNA repair (Figure S6A). Cells were exposed to ±7.5 Gy irradiation in the presence or absence of HGF (20 ng/mL). Four days later, cells were sorted by fluorescence-activated cell sorting (FACS) into fractions harboring low (MET^{low}) or high (MET^{high}) membrane MET expression (Figures 5A and 5B). The sorting threshold was defined using the median MET surface signal of non-irradiated controls (Figure S6B). Immunoblot analysis confirmed increased MET protein abundance in MET^{high} fractions compared to MET^{low} fractions (Figure S6C). To determine whether 5′ UTR-replacing fusion transcripts were present in these populations, we performed 5′ rapid amplification of cDNA ends (5′ RACE) using *MET*-specific reverse transcription (Figure 5A). Amplification products were cloned and sequenced. Fusion-positive transcripts were detected in MET^{high} populations following irradiation (Figure 5C). A greater number of fusion transcripts was observed in HGF-treated samples, consistent with survival advantage conferred by the ligand.[49,50] No fusion-positive transcripts were identified in MET^{low} fractions. A representative chromatogram illustrating a precise junction between a partner-derived 5′ UTR and the MET transcript is shown in Figure 5D, the corresponding fusion architectures in Figure 5E, and additional sequencing chromatograms in Figure S6E. All retained fusion transcript sequences align with annotated 5′ UTRs and show no mutations within the analyzed MET coding region. Notably, all partner-derived 5′ UTRs displayed lower composite 5′ UTR complexity scores, consistent with reduced structural and regulatory complexity (Figure 5F; Figure S6D). Functional testing of partner-derived 5′ UTRs in luciferase reporter assays demonstrated increased translational output relative to the native *MET* 5′ UTR (Figure 5G; Figures S6F and S6G). Together, these data show that 5′ UTR-replacing fusion transcripts can be detected following irradiation and that the identified partner-derived 5′ UTRs enhance translational output relative to the native *MET* 5′ UTR in reporter assays.

5′ UTR fusions generalize to oncogenes with complex untranslated regions

Building on the *MET* paradigm, we asked whether 5′ UTR-replacing fusions can be observed among other oncogenes. Consistent with previous observations,[51] a genome-wide comparison of 5′ UTRs revealed that the twenty-seven oncogenes analyzed contain more restrictive regulatory elements than other protein-coding genes. They have long 5′ UTRs, high GC content, uORFs, and complex secondary structures, resulting in an increased composite complexity score (Figures S7A–S7F). These features are all associated with translational repression, suggesting that the 5′ UTRs of oncogenes act as a translational "brake" limiting protein output. Cancer cells may bypass these regulatory elements through structural rearrangements.

To test this hypothesis, we analyzed fusion junction positions across these oncogenes (Table S8). We found that 5′ UTR-replacing fusions in cancer are not unique to *MET*; they are also observed in other cancer drivers, including *FGFR1*, *FGFR2*, *JAK2*, *NTRK2*, *PDGFRA*, *ETV1*, and *ETV4* (Figure S7G). RNA-sequencing support was detected for the vast majority of retained events (Table S9). Across fusion events, donor 5′ UTRs were predominantly simpler than the corresponding oncogene 5′ UTRs (Figure 6A; Figures S7H–S7L; Table S10). This pattern indicates that fusion events preferentially substitute restrictive 5′ UTRs with more translation-permissive ones. To functionally assess the translational impact of these partner-derived 5′ UTRs, we cloned selected 5′ UTRs from oncogenes or their fusion partners upstream of a NanoLuc reporter gene. As observed for *MET*, partner-derived 5′ UTRs markedly increased translational output relative to the native oncogene 5′ UTRs, while reporter mRNA levels remained largely unchanged (Figure 6B; Figures S8A–S8C).

To further analyze the consequences of UTR rewiring in a cellular context, we focused on two representative oncogenes: *ETV1* (encoding a transcription factor) and *FGFR1* (encoding a receptor tyrosine kinase). We engineered U2OS cells stably expressing *ETV1* driven either by its native 5′ UTR or by the partner-derived *MTFR1* 5′ UTR, and *FGFR1* driven by its native 5′ UTR or by the partner-derived *TEC* 5′ UTR. *MTFR1-ETV1* fusion led to a marked increase in ETV1 protein levels without corresponding changes in mRNA abundance (Figure 6C). Consistently, fusion-expressing cells displayed increased activation of an ETV1-responsive reporter and upregulation of endogenous ETV1 target genes (Figure 6D; Figures S8D–S8F). Similarly, *TEC-FGFR1* fusion-expressing cells increased FGFR1 protein expression while maintaining comparable mRNA levels (Figure 6E). This increase in receptor abundance resulted in heightened downstream signaling upon ligand (FGF2) stimulation, as evidenced by enhanced phosphorylation of FGFR1, FRS2, and ERK1/2, while remaining sensitive to pharmacological inhibition by the FGFR1 inhibitor AZD4547 (Figure 6F; Figure S8G).

Altogether, these results identify 5′ UTR-replacing fusions as a previously underappreciated class of oncogene fusion events that increase oncogene protein output by rewiring UTR regulation (Figure 6G).

DISCUSSION

Fusion genes have long been viewed as hybrid molecules with deregulated functions that drive oncogenesis.[1,3,15] Here, we define a distinct class of gene fusions that act not by altering protein structure, but by replacing the 5′ UTR of mRNA, a key element of translation efficiency. We term this mechanism UTR rewiring, a genetically encoded strategy that relieves translational repression and enhances oncogene expression, without modifying the protein itself.

The *MET* oncogene provides a compelling model for this phenomenon. We find that 34 of 182 evaluable *MET* fusion calls (18.7%) involve junction positions within the annotated *MET* 5′ UTR, preserving the full-length protein while replacing its native 5′ UTR. The biology of these 5′ UTR-replacing fusions has remained largely unexplored, often overlooked because the coding sequence is preserved. The *MET* 5′ UTR, far from being neutral, is enriched in features associated with translational repression: it is long, GC-rich, highly structured, and contains two experimentally validated uORFs, one of which is

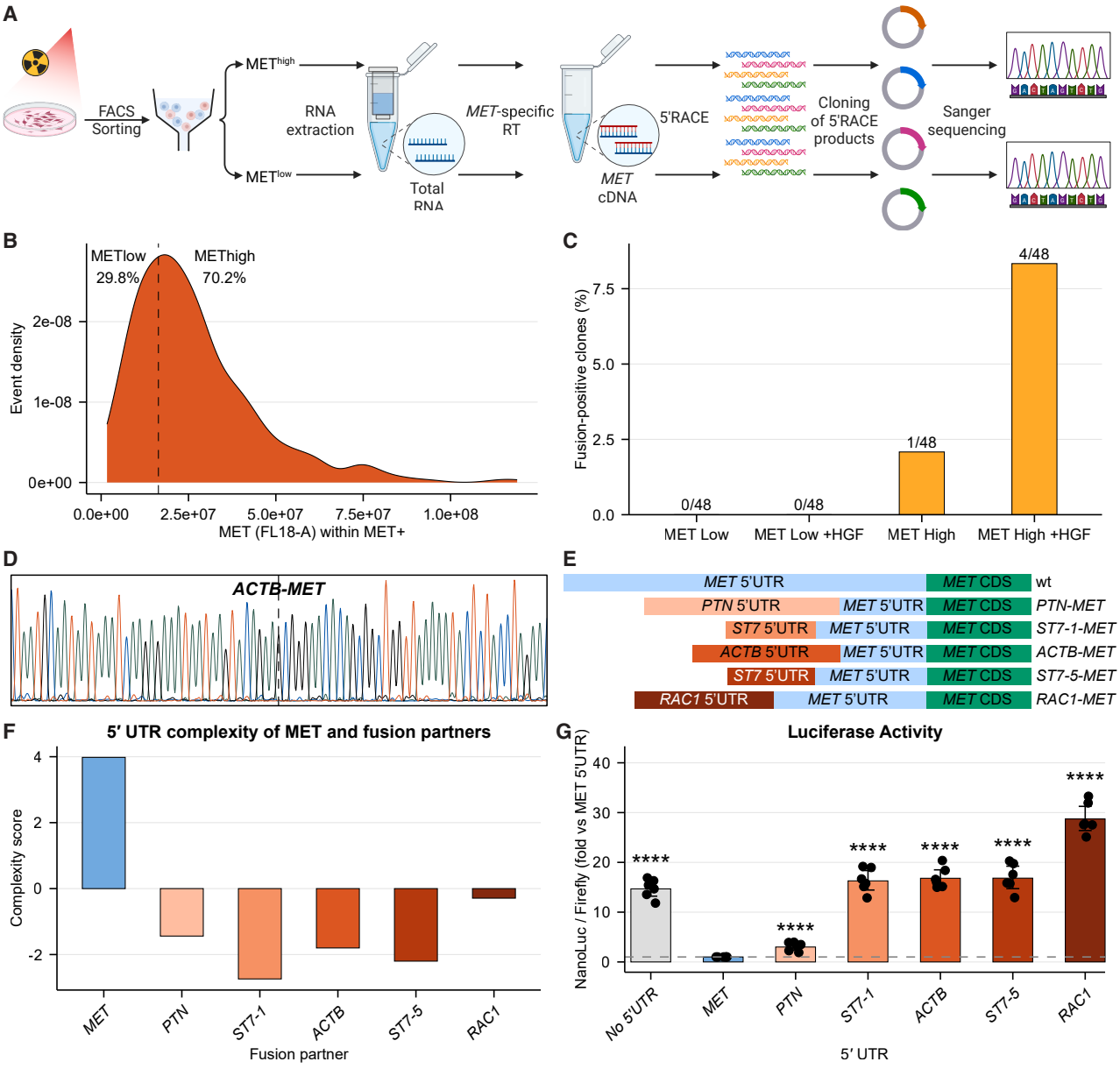


Figure 5. 5′ UTR-replacing MET fusion transcripts are detected in MET^{high} cells following irradiation

(A) Experimental workflow for identification of *MET* fusion transcripts by 5′ RACE. A172 cells were irradiated (±7.5 Gy) in the presence or absence of HGF (20 ng/mL) and cultured for four days. Cells were then sorted by FACS into MET^{high} and MET^{low} populations based on surface MET expression. Total RNA was extracted from each population and subjected to *MET*-specific reverse transcription to generate cDNA. 5′ RACE was performed to enrich and amplify the 5′ ends of *MET* transcripts. Amplified products were cloned and analyzed by Sanger sequencing to identify possible 5′ UTR-replacing fusion transcripts.

(B) Flow cytometry identifies a MET^{high} subpopulation in A172 cells four days after 7.5 Gy irradiation. Density plot generated from non-irradiated control cells is shown in Figure S6B. Data are representative of $n = 3$ independent biological experiments.

(C) 5′ RACE clones containing fusion transcripts in populations sorted based on surface MET expression. Fusion transcripts were detected in MET^{high} populations following irradiation, and a greater number of fusion-containing 5′ RACE clones was recovered in the presence of HGF. Numbers above bars indicate 5′ RACE clones containing fusion transcripts over total sequenced clones (48 clones per condition were sequenced across two independent 5′ RACE experiments).

(D) Representative Sanger chromatogram showing a 5′ UTR-replacing fusion transcript joining a partner-derived 5′ UTR to the *MET* coding sequence.

(E) Schematic representation of identified fusion architectures. In each case, a partner-derived 5′ UTR replaces the native *MET* 5′ UTR. Sequencing chromatograms are shown in Figure S6E. In each case, partner-derived sequence replaces all or part of the native MET 5′ UTR.

(F) Complexity scores of the native *MET* 5′ UTR and fusion partner 5′ UTRs as defined in STAR Methods.

(G) Luciferase reporter assays comparing translational output of native *MET* 5′ UTR and partner-derived 5′ UTRs. NanoLuc activity was normalized to firefly and expressed relative to the native *MET* 5′ UTR. Data represent mean ± SEM from $n = 6$ independent biological replicates. Statistics: one-way ANOVA with Dunnett's post hoc test vs. *MET* 5′ UTR (****$p < 0.0001$).

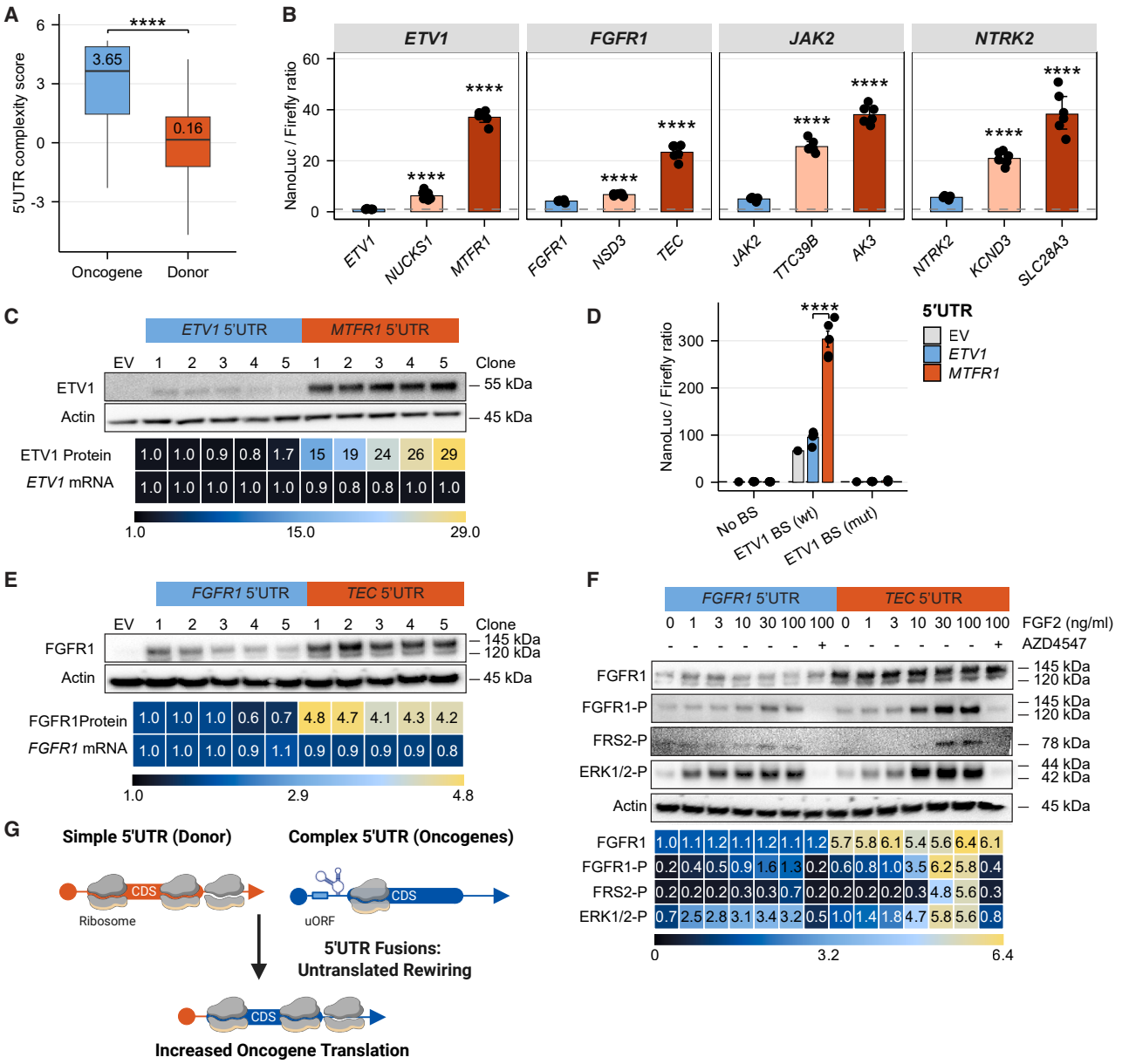


Figure 6. 5′ UTR fusions generalize to oncogenes with complex untranslated regions

(A) Boxplot comparing composite 5′ untranslated region (5′ UTR) complexity scores between the twenty-seven oncogenes analyzed and their fusion partner (donor) genes. Values within boxes correspond to median complexity scores of each group. Statistical significance was assessed using a two-sided paired Wilcoxon signed-rank test across oncogene-donor 5′ UTR pairs. ****$p < 0.0001$.

(B) NanoLuc reporter assays comparing translational output driven by native oncogene 5′ UTRs (*ETV1*, *FGFR1*, *JAK2*, and *NTRK2*) and corresponding partner-derived 5′ UTRs. The complete set of raw NanoLuc activities, including ETV4 and FGFR2, is shown in Figure S8A; corresponding firefly controls and NanoLuc mRNA levels are shown in Figures S8B and S8C, respectively. NanoLuc activity was normalized to firefly and expressed relative to the native oncogene 5′ UTR. Data represent mean ± SEM from $n = 6$ independent biological replicates. Statistical analysis: one-way ANOVA followed by Dunnett's post hoc test versus the native oncogene 5′ UTR. ****, $p < 0.0001$.

(C) Representative immunoblots of ETV1 protein levels in U2OS cells expressing constructs containing either the native *ETV1* 5′ UTR or the *MTFR1* partner-derived 5′ UTR. Five independent clones per construct are shown. Quantification (heatmap) shows densitometric protein levels normalized to actin. Empty vector-infected cells (EV, i.e., pLenti-mApple, see STAR Methods) are used as controls. The corresponding RT-qPCR analysis shows comparable *ETV1* mRNA levels across clones ($n = 3$ independent experiments).

(D) NanoLuc reporter assay of ETV1 transcriptional activity. Cells were transfected with a NanoLuc construct driven by ETV1 binding sites (ETV1 BS, WT) or matched controls lacking binding sites (no BS) or carrying mutated sites (ETV1 BS, mut). *MTFR1-ETV1* fusion cells showed increased NanoLuc activity with ETV1 BS (WT). Data represent mean ± SEM from $n = 5$ independent clones. Data were analyzed using a linear model including UTR × construct interaction, followed by emmeans contrasts with Holm correction. ****$p < 0.0001$.

(legend continued on next page)

independently annotated in the recently published TransCODE catalog of translated ORFs.[25–28] Its replacement results in elevated MET protein levels and enhanced cellular responsiveness to HGF, thereby promoting biological responses such as cell motility and survival following irradiation. Notably, the MET receptor remains structurally intact and ligand-dependent. Because the complete *MET* coding sequence is preserved, these fusions are not expected to alter the intrinsic biochemical properties of the receptor itself. Rather, the enhanced signaling observed following HGF stimulation is most parsimoniously explained by increased receptor abundance. Thus, the oncogenic phenotype does not require a gain-of-function alteration of the receptor but results from increased MET protein abundance following relief of 5′ UTR-mediated repression. These findings expand current models of oncogene activation by demonstrating that altered translational control alone can increase oncogenic protein output.

At the mechanistic level, these fusions function by replacing a translationally restrictive 5′ UTR with a partner-derived sequence corresponding to an annotated 5′ UTR that is generally shorter, less structured, and depleted in uORFs—a configuration associated with more efficient translation initiation.[25–27] Our prior work demonstrated that the *MET* 5′ UTR serves as a stress-responsive translational control element, tightly controlling protein output.[29] Here, we show that this regulatory layer can be genetically bypassed via 5′ UTR replacement, a genetically encoded route to oncogene overexpression without corresponding changes in mRNA abundance. This logic extends beyond *MET*. Across more than 200,000 profiled cancer samples,[24] we identify similar 5′ UTR-replacing fusion calls in other oncogenes. These genes share native 5′ UTRs enriched in features commonly associated with translational repression. In contrast, the annotated 5′ UTRs of their fusion partners display simpler features associated with more efficient translation. These findings suggest that integrating 5′ UTR structural features into fusion annotation frameworks may enhance the identification of clinically relevant rearrangements.

The functional consequences described here should also be considered in the broader context of physiological mechanisms that modulate translation through alternative 5′ UTRs, including alternative promoter usage, alternative transcription start sites, alternative first-exon selection, and alternative splicing. These processes generate transcript isoforms with distinct 5′ UTRs while preserving the same protein-coding sequence, thereby modulating translational efficiency through changes in 5′ UTR architecture and regulatory features.[52,53] In contrast, UTR rewiring represents a genetically encoded counterpart to these physiological mechanisms, in which these fusion events replace the native 5′ UTR with partner-derived non-coding sequences while preserving the encoded protein.

Early observations by Marilyn Kozak noted that many oncogenes possess unusually complex 5′ UTRs, likely serving as an evolutionary brake on aberrant expression.[51] In this light, UTR rewiring emerges as a strategy for cancers to bypass this regulatory constraint. While transcriptional upregulation, enhancer hijacking, and copy number amplification are well documented, the role of UTR-mediated translational control remains underexplored.[54–57] Yet, multiple high-throughput approaches—including ribosome profiling, proteogenomics, and spatial transcriptomics—increasingly reveal that mRNA abundance is a poor proxy for protein output.[58–61] Our findings provide a mechanistic explanation for this uncoupling: 5′ UTR-replacing fusion events can bypass repressive 5′ UTRs and unleash oncogene expression at the level of translation. Together with our recent findings on the inducible nature of *MET* translation,[29] this study offers a complementary, genetically encoded route to protein dosage magnification.

Functionally, 5′ UTR-replacing fusions behave as dosage-enhancing lesions, increasing the abundance of the WT oncogene. In *MET*, this overexpression enhances cellular responsiveness to HGF, promoting invasive growth and survival following genotoxic stress. The detection of these fusion transcripts following irradiation raises the possibility that UTR rewiring may provide a selective advantage under hostile microenvironmental conditions. This model is also consistent with recent clinical observations that many kinase-domain-intact *MET* fusions are detected after therapy and may initially exist as subclonal events.[62] Whether these fusions arose following treatment or were already present as rare subclonal events that subsequently expanded remains to be determined. Together, these observations support the hypothesis that MET signaling may contribute to adaptive responses following genotoxic stress, consistent with previous studies demonstrating a role for MET in radioresistance.[29,44,63] Further work will be required to determine whether 5′ UTR-replacing fusions influence therapeutic responses *in vivo* and whether they define patient subsets that could benefit from MET-targeted strategies.

To date, 5′UTR replacements have been largely overlooked and remain inconsistently annotated in clinical genomics datasets. Most fusion-calling algorithms prioritize disruptions of the coding sequences that create chimeric proteins.[64,65] Rearrangements that preserve the open reading frame and affect only the 5′UTR are typically filtered out or dismissed as neutral. This assumption is both surprising and historically inconsistent. Decades ago, studies on the *FOS* oncogene demonstrated that replacing non-coding regulatory sequences alone—particularly the 3′ UTR—was sufficient to endow the proto-oncogene

(E) U2OS cells expressing either WT *FGFR1* or *TEC-FGFR1* fusion. Western blot and RT-qPCR analyses show increased FGFR1 protein levels despite comparable mRNA abundance ($n = 5$ independent clones).

(F) Cells expressing either WT *FGFR1* or *TEC-FGFR1* fusion were stimulated with increasing concentrations of FGF2 in the presence or absence of the FGFR inhibitor AZD4547 (500 nM). Immunoblots show total FGFR1, p-FGFR1, and signal transducers (p-FRS2 and p-ERK1/2). Representative of $n = 3$ independent biological experiments.

(G) Schematic model illustrating the mechanism of 5′ UTR fusion-driven translational activation. Oncogenes typically harbor complex 5′ UTRs that inhibit translation. 5′ UTR fusions remove these inhibitory elements by replacing the repressive 5′ UTR with a simpler sequence, thereby enhancing cap-dependent translation and oncogene expression—a process termed UTR rewiring.

with transforming potential.[66,67] In a disease as complex as cancer, such simplifications—considering UTRs as inert—are no longer tenable. Our data challenge this view and call for a revision of fusion annotation frameworks, adding new layers for patient stratification.

By revealing a mechanism through which protein output is genetically increased via 5′ UTR replacement, this work underscores the regulatory power embedded in the untranslated genome. In this light, UTR rewiring emerges as a functionally significant force in cancer—one that acts not by altering the message, but by amplifying how efficiently it is read.

Limitations of the study

Several limitations of this study should be acknowledged. First, the composite 5′ UTR complexity score was designed to provide a descriptive summary of several established determinants of translation efficiency, rather than a comprehensive or predictive model of translational regulation. As an unweighted linear metric, it does not capture non-linear or interdependent effects among features: GC content and predicted folding stability are correlated, while uORF count does not account for uORF position, initiation context, or inhibitory strength. Additional cis-regulatory properties, including RNA-binding protein interactions, RNA modifications, and sequence motifs, are also likely to influence protein output. Moreover, RNA secondary structure was estimated using minimum-free-energy predictions, which provide only a computational approximation of RNA folding *in vivo*. Second, because most *MET* fusion calls in GENIE are supported by RNA sequencing, these data establish the presence of chimeric transcripts but do not independently demonstrate the underlying genomic rearrangement in every case. The type of supporting evidence available for each event is reported in Table S4. Third, the irradiation/5′ RACE experiment establishes that 5′ UTR-replacing *MET* fusion transcripts can be detected in MET^{high} populations following irradiation, but it does not determine their contribution to increased surface MET expression. Because the analysis was performed on RNA extracted from lysed sorted populations, the cells giving rise to the individual fusion transcripts were no longer available for matched genomic characterization. Consequently, this analysis cannot identify the corresponding DNA breakpoints or determine whether *MET* copy-number alterations or other mechanisms of *MET* overexpression coexist within the fusion-positive cells. It also cannot distinguish between *de novo* fusion formation following irradiation and the enrichment of rare pre-existing fusion-bearing clones. Fourth, although the causal contribution of 5′ UTR replacement was established in matched experimental systems, future studies will be required to determine the therapeutic relevance of UTR rewiring across tumor types and to establish whether patients harboring these fusions may derive a particular benefit from targeted therapies. Finally, our study establishes the functional consequences of 5′ UTR replacement but does not address the molecular mechanisms responsible for generating these rearrangements. Determining how UTR rewiring arises during tumor evolution, and under which selective pressures it is favored, represents an important direction for future investigation.

RESOURCE AVAILABILITY

Lead contact

Requests for further information and resources should be directed to and will be fulfilled by the lead contact, Dogus M Altintas (dogus.altintas@gmail.com).

Materials availability

All plasmids generated in this study have been deposited at Addgene and are listed in the key resources table with their corresponding Addgene accession numbers.

All stable cell lines generated in this study are available from the lead contact upon reasonable request without restriction.

Data and code availability

- This paper analyzes publicly available cancer genomics datasets from AACR Project GENIE (v17.0-public) and TCGA. These resources are listed in the key resources table.
- Source data, uncropped western blots, raw 5′ RACE sequencing data, processed datasets, R scripts, session information files, and all computational resources required to reproduce the analyses have been deposited at Zenodo and are publicly available as of the date of publication at https://doi.org/10.5281/zenodo.21804107.
- Any additional information required to reanalyze the data reported in this paper is available from the lead contact upon request.

ACKNOWLEDGMENTS

We are grateful to Romain Charton for insightful discussions and Héloïse Altintas for assistance with illustrations. We also thank the IFOM Cell Biology Unit (RRID: SCR_026864), IFOM Imaging Unit (RRID: SCR_026866), Cogentech DNA Sanger Sequencing Core Facility (RRID: SCR_026939), Cogentech Quantitative PCR Service (RRID: SCR_026936), and Cogentech Genomics Core Facility (RRID: SCR_026935) for technical assistance. All illustrations were created with BioRender.com. This work was supported by the Associazione Italiana per la Ricerca sul Cancro (AIRC, grant no. 23820 to P.M.C.) and by the Fondazione Umberto Veronesi (FUV, grant no. 3916 to D.M.A.). We dedicate this work to the memory of Dr Daigo Sawaki (July 1973–February 2026), our former colleague and collaborator, whose passion for science and generosity deeply inspired us.

AUTHOR CONTRIBUTIONS

Conceptualization, D.M.A. and P.M.C.; methodology, D.M.A. and P.M.C.; investigation, D.M.A., M.C., E.B., and C.C.; formal analysis, D.M.A.; visualization, D.M.A.; writing – original draft, D.M.A. and P.M.C.; writing – review and editing, D.M.A. and P.M.C.; supervision, D.M.A. and P.M.C.; funding acquisition, D.M.A. and P.M.C.

DECLARATION OF INTERESTS

The authors declare no competing interests.

STAR★METHODS

Detailed methods are provided in the online version of this paper and include the following:

- KEY RESOURCES TABLE
- EXPERIMENTAL MODEL AND STUDY PARTICIPANT DETAILS
- METHOD DETAILS
  - Computational analysis
  - Cell culture and treatments
  - Generation of stable cell lines
  - Western blotting
  - Polysome profiling
  - Cycloheximide chase assay
  - Nucleic acid extraction and qPCR

- Immunofluorescence
- Cell surface MET detection by flow cytometry
- NanoLuc reporter assay
- Irradiation and survival assays
- Wound healing assay
- 5′ rapid amplification of cDNA ends (5′RACE)

- QUANTIFICATION AND STATISTICAL ANALYSIS
  - Additional resources

SUPPLEMENTAL INFORMATION

Supplementary data related to this article can be found online at https://doi.org/10.1016/j.celrep.2026.118145.

Received: June 16, 2026
Revised: August 6, 2026
Accepted: September 25, 2026

REFERENCES

1. Hanahan, D., and Weinberg, R.A. (2011). Hallmarks of cancer: the next generation. Cell *144*, 646–674. https://doi.org/10.1016/j.cell.2011.02.013.
2. Mertens, F., Johansson, B., Fioretos, T., and Mitelman, F. (2015). The emerging complexity of gene fusions in cancer. Nat. Rev. Cancer *15*, 371–381. https://doi.org/10.1038/nrc3947.
3. Mitelman, F., Johansson, B., and Mertens, F. (2007). The impact of translocations and gene fusions on cancer causation. Nat. Rev. Cancer *7*, 233–245. https://doi.org/10.1038/nrc2091.
4. Li, J., Lu, H., Ng, P.K.S., Pantazi, A., Ip, C.K.M., Jeong, K.J., Amador, B., Tran, R., Tsang, Y.H., Yang, L., et al. (2022). A functional genomic approach to actionable gene fusions for precision oncology. Sci. Adv. *8*, eabm2382. https://doi.org/10.1126/sciadv.abm2382.
5. Futreal, P.A., Coin, L., Marshall, M., Down, T., Hubbard, T., Wooster, R., Rahman, N., and Stratton, M.R. (2004). A census of human cancer genes. Nat. Rev. Cancer *4*, 177–183. https://doi.org/10.1038/nrc1299.
6. Salokas, K., Weldatsadik, R.G., and Varjosalo, M. (2020). Human transcription factor and protein kinase gene fusions in human cancer. Sci. Rep. *10*, 14169. https://doi.org/10.1038/s41598-020-71040-8.
7. Lipson, D., Capelletti, M., Yelensky, R., Otto, G., Parker, A., Jarosz, M., Curran, J.A., Balasubramanian, S., Bloom, T., Brennan, K.W., et al. (2012). Identification of new ALK and RET gene fusions from colorectal and lung cancer biopsies. Nat. Med. *18*, 382–384. https://doi.org/10.1038/nm.2673.
8. Liu, S.V., Nagasaka, M., Atz, J., Solca, F., and Müllauer, L. (2025). Oncogenic gene fusions in cancer: from biology to therapy. Signal Transduct. Target. Ther. *10*, 111. https://doi.org/10.1038/s41392-025-02161-7.
9. Rowley, J.D. (1973). Letter: A new consistent chromosomal abnormality in chronic myelogenous leukaemia identified by quinacrine fluorescence and Giemsa staining. Nature *243*, 290–293. https://doi.org/10.1038/243290a0.
10. Daley, G.Q., Van Etten, R.A., and Baltimore, D. (1990). Induction of chronic myelogenous leukemia in mice by the P210bcr/abl gene of the Philadelphia chromosome. Science *247*, 824–830. https://doi.org/10.1126/science.2406902.
11. Grieco, M., Santoro, M., Berlingieri, M.T., Melillo, R.M., Donghi, R., Bongarzone, I., Pierotti, M.A., Della Ports, G., Fusco, A., and Vecchiot, G. (1990). PTC is a novel rearranged form of the ret proto-oncogene and is frequently detected in vivo in human thyroid papillary carcinomas. Cell *60*, 557–563. https://doi.org/10.1016/0092-8674(90)90659-3.
12. Kohno, T., Ichikawa, H., Totoki, Y., Yasuda, K., Hiramoto, M., Nammo, T., Sakamoto, H., Tsuta, K., Furuta, K., Shimada, Y., et al. (2012). KIF5B-RET fusions in lung adenocarcinoma. Nat. Med. *18*, 375–377. https://doi.org/10.1038/nm.2644.
13. Morris, S.W., Kirstein, M.N., Valentine, M.B., Dittmer, K., Shapiro, D.N., Look, A.T., and Saltman, D.L. (1995). Fusion of a kinase gene, ALK, to a nucleolar protein gene, NPM, in non-Hodgkin's lymphoma. Science *267*, 316–317. https://doi.org/10.1126/science.267.5196.316-b.
14. Soda, M., Choi, Y.L., Enomoto, M., Takada, S., Yamashita, Y., Ishikawa, S., Fujiwara, S.i., Watanabe, H., Kurashina, K., Hatanaka, H., et al. (2007). Identification of the transforming EML4-ALK fusion gene in non-small-cell lung cancer. Nature *448*, 561–566. https://doi.org/10.1038/nature05945.
15. Testa, J.R., Park, M., Blair, D.G., Kalbakji, A., Arden, K., and Vande Woude, G.F. (1990). Analysis by pulsed field gel electrophoresis reveals complex rearrangements in two MET alleles in a chemically-treated human cell line, MNNG-HOS. Oncogene *5*, 1565–1571.
16. Febres-Aldana, C.A., Vojnic, M., Odintsov, I., Zhang, T., Cheng, R., Beach, C.Z., Lu, D., Mattar, M.S., Gazzo, A.M., Gili, L., et al. (2025). Pan-Cancer Analysis of Oncogenic MET Fusions Reveals Distinct Pathogenomic Subsets with Differential Sensitivity to MET-Targeted Therapy. Cancer Discov. *15*, 1141–1158. https://doi.org/10.1158/2159-8290.Cd-24-0417.
17. Birchmeier, C., Birchmeier, W., Gherardi, E., and Vande Woude, G.F. (2003). Met, metastasis, motility and more. Nat. Rev. Mol. Cell Biol. *4*, 915–925. https://doi.org/10.1038/nrm1261.
18. Boccaccio, C., and Comoglio, P.M. (2006). Invasive growth: a MET-driven genetic programme for cancer and stem cells. Nat. Rev. Cancer *6*, 637–645. https://doi.org/10.1038/nrc1912.
19. Comoglio, P.M., Trusolino, L., and Boccaccio, C. (2018). Known and novel roles of the MET oncogene in cancer: a coherent approach to targeted therapy. Nat. Rev. Cancer *18*, 341–358. https://doi.org/10.1038/s41568-018-0002-y.
20. Gherardi, E., Birchmeier, W., Birchmeier, C., and Woude, G.V. (2012). Targeting MET in cancer: rationale and progress. Nat. Rev. Cancer *12*, 89–103. https://doi.org/10.1038/nrc3205.
21. Vigna, E., Gramaglia, D., Longati, P., Bardelli, A., and Comoglio, P.M. (1999). Loss of the exon encoding the juxtamembrane domain is essential for the oncogenic activation of TPR-MET. Oncogene *18*, 4275–4281. https://doi.org/10.1038/sj.onc.1202791.
22. Gow, C.H., Liu, Y.N., Li, H.Y., Hsieh, M.S., Chang, S.H., Luo, S.C., Tsai, T.H., Chen, P.L., Tsai, M.F., and Shih, J.Y. (2018). Oncogenic Function of a KIF5B-MET Fusion Variant in Non-Small Cell Lung Cancer. Neoplasia *20*, 838–847. https://doi.org/10.1016/j.neo.2018.06.007.
23. Nakazawa, S., Pecci, F., Odintsov, I., Gazgalis, D., Gottlieb, F.H., Ricciuti, B., Zullo, L., Alessi, J.V., Di Federico, A., Aldea, M., et al. (2025). Antitumor Activity of Vebreltinib and Characterization of Clinicogenomic Features in Solid Tumors with MET Rearrangements. Cancer Discov. *15*, 1129–1140. https://doi.org/10.1158/2159-8290.Cd-24-1726.
24. AACR Project GENIE Consortium (2017). AACR Project GENIE: Powering Precision Medicine through an International Consortium. Cancer Discov. *7*, 818–831. https://doi.org/10.1158/2159-8290.Cd-17-0151.
25. Hinnebusch, A.G., Ivanov, I.P., and Sonenberg, N. (2016). Translational control by 5′-untranslated regions of eukaryotic mRNAs. Science *352*, 1413–1416. https://doi.org/10.1126/science.aad9868.
26. Kertesz, M., Wan, Y., Mazor, E., Rinn, J.L., Nutter, R.C., Chang, H.Y., and Segal, E. (2010). Genome-wide measurement of RNA secondary structure in yeast. Nature *467*, 103–107. https://doi.org/10.1038/nature09322.
27. Johnstone, T.G., Bazzini, A.A., and Giraldez, A.J. (2016). Upstream ORFs are prevalent translational repressors in vertebrates. Embo j *35*, 706–723. https://doi.org/10.15252/embj.201592759.
28. Chothani, S., Ruiz-Orera, J., Tierney, J.A.S., Swirski, M.I., Tjeldnes, H., Kok, L.W., Clauwaert, J., Deutsch, E.W., Alba, M.M., Aspden, J.L., et al. (2026). An expanded reference catalog of translated open reading frames for biomedical research. Nucleic Acids Res. *54*, gkag234. https://doi.org/10.1093/nar/gkag234.

29. Cerqua, M., Foiani, M., Boccaccio, C., Comoglio, P.M., and Altintas, D.M. (2025). The integrated stress response drives MET oncogene overexpression in cancers. Embo j *44*, 6. https://doi.org/10.1038/s44318-024-00338-4.

30. Calvo, S.E., Pagliarini, D.J., and Mootha, V.K. (2009). Upstream open reading frames cause widespread reduction of protein expression and are polymorphic among humans. Proc. Natl. Acad. Sci. USA *106*, 7507–7512. https://doi.org/10.1073/pnas.0810916106.

31. Kozak, M. (1986). Influences of mRNA secondary structure on initiation by eukaryotic ribosomes. Proc. Natl. Acad. Sci. USA *83*, 2850–2854. https://doi.org/10.1073/pnas.83.9.2850.

32. Lorenz, R., Bernhart, S.H., Höner Zu Siederdissen, C., Tafer, H., Flamm, C., Stadler, P.F., and Hofacker, I.L. (2011). ViennaRNA Package 2.0. Algorithms Mol. Biol. *6*, 26. https://doi.org/10.1186/1748-7188-6-26.

33. Ghandi, M., Huang, F.W., Jané-Valbuena, J., Kryukov, G.V., Lo, C.C., McDonald, E.R., III, Barretina, J., Gelfand, E.T., Bielski, C.M., Li, H., et al. (2019). Next-generation characterization of the Cancer Cell Line Encyclopedia. Nature *569*, 503–508. https://doi.org/10.1038/s41586-019-1186-3.

34. Arafeh, R., Shibue, T., Dempster, J.M., Hahn, W.C., and Vazquez, F. (2025). The present and future of the Cancer Dependency Map. Nat. Rev. Cancer *25*, 59–73. https://doi.org/10.1038/s41568-024-00763-x.

35. Bottaro, D.P., Rubin, J.S., Faletto, D.L., Chan, A.M.L., Kmiecik, T.E., Vande Woude, G.F., and Aaronson, S.A. (1991). Identification of the hepatocyte growth factor receptor as the c-met proto-oncogene product. Science *251*, 802–804. https://doi.org/10.1126/science.1846706.

36. Trusolino, L., and Comoglio, P.M. (2002). Scatter-factor and semaphorin receptors: cell signalling for invasive growth. Nat. Rev. Cancer *2*, 289–300. https://doi.org/10.1038/nrc779.

37. Apicella, M., Giannoni, E., Fiore, S., Ferrari, K.J., Fernández-Pérez, D., Isella, C., Granchi, C., Minutolo, F., Sottile, A., Comoglio, P.M., et al. (2018). Increased Lactate Secretion by Cancer Cells Sustains Non-cell-autonomous Adaptive Resistance to MET and EGFR Targeted Therapies. Cell Metab. *28*, 848–865.e6. https://doi.org/10.1016/j.cmet.2018.08.006.

38. Altintas, D.M., and Comoglio, P.M. (2023). An Observatory for the MET Oncogene: A Guide for Targeted Therapies. Cancers (Basel) *15*, 4672. https://doi.org/10.3390/cancers15184672.

39. Petrini, I. (2015). Biology of MET: a double life between normal tissue repair and tumor progression. Ann. Transl. Med. *3*, 82. https://doi.org/10.3978/j.issn.2305-5839.2015.03.58.

40. Peschard, P., Fournier, T.M., Lamorte, L., Naujokas, M.A., Band, H., Langdon, W.Y., and Park, M. (2001). Mutation of the c-Cbl TKB domain binding site on the Met receptor tyrosine kinase converts it into a transforming protein. Mol. Cell *8*, 995–1004. https://doi.org/10.1016/s1097-2765(01)00378-1.

41. Mathieu, L.N., Larkins, E., Akinboro, O., Roy, P., Amatya, A.K., Fiero, M.H., Mishra-Kalyani, P.S., Helms, W.S., Myers, C.E., Skinner, A.M., et al. (2022). FDA Approval Summary: Capmatinib and Tepotinib for the Treatment of Metastatic NSCLC Harboring MET Exon 14 Skipping Mutations or Alterations. Clin. Cancer Res. *28*, 249–254. https://doi.org/10.1158/1078-0432.Ccr-21-1566.

42. Mak, H.H.L., Peschard, P., Lin, T., Naujokas, M.A., Zuo, D., and Park, M. (2007). Oncogenic activation of the Met receptor tyrosine kinase fusion protein, Tpr-Met, involves exclusion from the endocytic degradative pathway. Oncogene *26*, 7213–7221. https://doi.org/10.1038/sj.onc.1210522.

43. Bussolino, F., Di Renzo, M.F., Ziche, M., Bocchietto, E., Olivero, M., Naldini, L., Gaudino, G., Tamagnone, L., Coffer, A., and Comoglio, P.M. (1992). Hepatocyte growth factor is a potent angiogenic factor which stimulates endothelial cell motility and growth. J. Cell Biol. *119*, 629–641. https://doi.org/10.1083/jcb.119.3.629.

44. De Bacco, F., Luraghi, P., Medico, E., Reato, G., Girolami, F., Perera, T., Gabriele, P., Comoglio, P.M., and Boccaccio, C. (2011). Induction of MET by ionizing radiation and its role in radioresistance and invasive growth of cancer. J Natl Cancer Inst *103*, 645–661. https://doi.org/10.1093/jnci/djr093.

45. Zhou, D., Tan, R.J., Lin, L., Zhou, L., and Liu, Y. (2013). Activation of hepatocyte growth factor receptor, c-met, in renal tubules is required for renoprotection after acute kidney injury. Kidney Int. *84*, 509–520. https://doi.org/10.1038/ki.2013.102.

46. Jeffers, M., Rong, S., and Vande Woude, G.F. (1996). Hepatocyte growth factor/scatter factor-Met signaling in tumorigenicity and invasion/metastasis. J. Mol. Med. *74*, 505–513. https://doi.org/10.1007/BF00204976.

47. Stella, M., and Comoglio, P.M. (1999). HGF: a multifunctional growth factor controlling cell scattering. Int. J. Biochem. Cell Biol. *31*, 1357–1362. https://doi.org/10.1016/s1357-2725(99)00089-8.

48. Gherardi, E., Sandin, S., Petoukhov, M.V., Finch, J., Youles, M.E., Öfverstedt, L.-G., Miguel, R.N., Blundell, T.L., Vande Woude, G.F., Skoglund, U., and Svergun, D.I. (2006). Structural basis of hepatocyte growth factor/scatter factor and MET signalling. Proc. Natl. Acad. Sci. USA *103*, 4046–4051. https://doi.org/10.1073/pnas.0509040103.

49. Bowers, D.C., Fan, S., Walter, K.A., Abounader, R., Williams, J.A., Rosen, E.M., and Laterra, J. (2000). Scatter Factor/Hepatocyte Growth Factor Protects against Cytotoxic Death in Human Glioblastoma via Phosphatidylinositol 3-Kinase- and AKT-dependent Pathways. Cancer Res. *60*, 4277–4283.

50. Lal, B., Xia, S., Abounader, R., and Laterra, J. (2005). Targeting the c-Met pathway potentiates glioblastoma responses to gamma-radiation. Clin. Cancer Res. *11*, 4479–4486. https://doi.org/10.1158/1078-0432.Ccr-05-0166.

51. Kozak, M. (1987). An analysis of 5'-noncoding sequences from 699 vertebrate messenger RNAs. Nucleic Acids Res. *15*, 8125–8148. https://doi.org/10.1093/nar/15.20.8125.

52. Tamarkin-Ben-Harush, A., Vasseur, J.-J., Debart, F., Ulitsky, I., and Dikstein, R. (2017). Cap-proximal nucleotides via differential eIF4E binding and alternative promoter usage mediate translational response to energy stress. eLife *6*, e21907. https://doi.org/10.7554/eLife.21907.

53. Weber, R., Ghoshdastider, U., Spies, D., Duré, C., Valdivia-Francia, F., Forny, M., Ormiston, M., Renz, P.F., Taborsky, D., Yigit, M., et al. (2023). Monitoring the 5′UTR landscape reveals isoform switches to drive translational efficiencies in cancer. Oncogene *42*, 638–650. https://doi.org/10.1038/s41388-022-02578-2.

54. Mansour, M.R., Abraham, B.J., Anders, L., Berezovskaya, A., Gutierrez, A., Durbin, A.D., Etchin, J., Lawton, L., Sallan, S.E., Silverman, L.B., et al. (2014). Oncogene regulation. An oncogenic super-enhancer formed through somatic mutation of a noncoding intergenic element. Science *346*, 1373–1377. https://doi.org/10.1126/science.1259037.

55. Beroukhim, R., Mermel, C.H., Porter, D., Wei, G., Raychaudhuri, S., Donovan, J., Barretina, J., Boehm, J.S., Dobson, J., Urashima, M., et al. (2010). The landscape of somatic copy-number alteration across human cancers. Nature *463*, 899–905. https://doi.org/10.1038/nature08822.

56. Dubois, F., Sidiropoulos, N., Weischenfeldt, J., and Beroukhim, R. (2022). Structural variations in cancer and the 3D genome. Nat. Rev. Cancer *22*, 533–546. https://doi.org/10.1038/s41568-022-00488-9.

57. Wang, X., and Yue, F. (2024). Hijacked enhancer-promoter and silencer-promoter loops in cancer. Curr. Opin. Genet. Dev. *86*, 102199. https://doi.org/10.1016/j.gde.2024.102199.

58. Hsieh, A.C., Liu, Y., Edlind, M.P., Ingolia, N.T., Janes, M.R., Sher, A., Shi, E.Y., Stumpf, C.R., Christensen, C., Bonham, M.J., et al. (2012). The translational landscape of mTOR signalling steers cancer initiation and metastasis. Nature *485*, 55–61. https://doi.org/10.1038/nature10912.

59. Keren, L., Bosse, M., Marquez, D., Angoshtari, R., Jain, S., Varma, S., Yang, S.R., Kurian, A., Van Valen, D., West, R., et al. (2018). A Structured Tumor-Immune Microenvironment in Triple Negative Breast Cancer

Revealed by Multiplexed Ion Beam Imaging. Cell *174*, 1373–1387.e19. https://doi.org/10.1016/j.cell.2018.08.039.

60. Cable, D.M., Murray, E., Zou, L.S., Goeva, A., Macosko, E.Z., Chen, F., and Irizarry, R.A. (2022). Robust decomposition of cell type mixtures in spatial transcriptomics. Nat. Biotechnol. *40*, 517–526. https://doi.org/10.1038/s41587-021-00830-w.
61. Tebaldi, T., Re, A., Viero, G., Pegoretti, I., Passerini, A., Blanzieri, E., and Quattrone, A. (2012). Widespread uncoupling between transcriptome and translatome variations after a stimulus in mammalian cells. BMC Genom. *13*, 220. https://doi.org/10.1186/1471-2164-13-220.
62. Jin, B., Ma, Y., Wu, Q., Ou, Q., Shao, Y., and Xu, S. (2024). Clinical and genomic analysis of baseline and acquired MET fusions with an intact kinase domain in lung cancer patients. Genes Dis. *11*, 76–79. https://doi.org/10.1016/j.gendis.2023.02.046.
63. Guryanova, O.A., and Bao, S. (2011). How scatter factor receptor c-MET contributes to tumor radioresistance: ready, set, scatter. J Natl Cancer Inst *103*, 617–619. https://doi.org/10.1093/jnci/djr103.
64. Uhrig, S., Ellermann, J., Walther, T., Burkhardt, P., Fröhlich, M., Hutter, B., Toprak, U.H., Neumann, O., Stenzinger, A., Scholl, C., et al. (2021). Accurate and efficient detection of gene fusions from RNA sequencing data. Genome Res. *31*, 448–460. https://doi.org/10.1101/gr.257246.119.
65. Dorney, R., Dhungel, B.P., Rasko, J.E.J., Hebbard, L., and Schmitz, U. (2023). Recent advances in cancer fusion transcript detection. Brief. Bioinform. *24*, bbac519. https://doi.org/10.1093/bib/bbac519.
66. Veyrune, J.L., Carillo, S., Vié, A., and Blanchard, J.M. (1995). c-fos mRNA instability determinants present within both the coding and the 3' non coding region link the degradation of this mRNA to its translation. Oncogene *11*, 2127–2134.
67. Lee, W.M.F., Lin, C., and Curran, T. (1988). Activation of the transforming potential of the human fos proto-oncogene requires message stabilization and results in increased amounts of partially modified fos protein. Mol. Cell Biol. *8*, 5521–5527. https://doi.org/10.1128/mcb.8.12.5521-5527.1988.
68. Jaako, P., Faille, A., Tan, S., Wong, C.C., Escudero-Urquijo, N., Castro-Hartmann, P., Wright, P., Hilcenko, C., Adams, D.J., and Warren, A.J. (2022). eIF6 rebinding dynamically couples ribosome maturation and translation. Nat. Commun. *13*, 1562. https://doi.org/10.1038/s41467-022-29214-7.

STAR★METHODS

KEY RESOURCES TABLE

REAGENT or RESOURCE	SOURCE	IDENTIFIER
Antibodies		
P-MET-Y1234/1235	Cell Signaling Technology	Cat# 3077; RRID: AB_2143886
Total MET	Cell Signaling Technology	Cat# 3148; RRID: AB_2143834
Total MET	R&D Systems	Cat# AF276; RRID: AB_355289
MET-PE	R&D Systems	Cat# FAB3582P; RRID: AB_357005
gamma-H2AX-S139	Cell Signaling Technology	Cat# 9718; RRID: AB_2118009
H3-HRP	Abcam	Cat# ab21054; RRID: AB_446995
Actin-HRP	Abcam	Cat# ab207674; RRID: AB_2868347
P-AKT-S473	Cell Signaling Technology	Cat# 9271; RRID: AB_329825
Total AKT	Cell Signaling Technology	Cat# 9272; RRID: AB_329827
ERK1/2-P-T202/Y204	Cell Signaling Technology	Cat# 9101; RRID: AB_331646
Total ERK1/2	Cell Signaling Technology	Cat# 9102; RRID: AB_330744
c-Myc	Abcam	Cat# ab32072; RRID: AB_731658
E-Cadherin	Abcam	Cat# ab40772; RRID: AB_731504
ACTA2	Sigma-Aldrich	Cat# A2547; RRID: AB_476701
ETV1	Abcam	Cat# ab314874
FGFR1	Cell Signaling Technology	Cat# 9740; RRID: AB_11178516
P-FGFR1-Y653/654	Cell Signaling Technology	Cat# 52928; RRID: AB_2799398
FRS2-P-Y436	Cell Signaling Technology	Cat# 3861; RRID: AB_2092546
Anti-rabbit IgG-HRP	Cell Signaling Technology	Cat# 7074; RRID: AB_2099233
Anti-mouse IgG-HRP	Cell Signaling Technology	Cat# 7076; RRID: AB_330924
Anti-goat IgG-AlexaFluor 488	Thermo Fisher Scientific	Cat# A11055; RRID: AB_2534102
Anti-rabbit IgG-AlexaFluor 647	Thermo Fisher Scientific	Cat# A21245; RRID: AB_2535813
Anti-mouse IgG-AlexaFluor 555	Thermo Fisher Scientific	Cat# A21422; RRID: AB_2535844
Chemicals, peptides, and recombinant proteins		
Recombinant human HGF	R&D Systems	Cat# 294-HGN/CF

(*Continued on next page*)

Continued

REAGENT or RESOURCE	SOURCE	IDENTIFIER
Recombinant human FGF2	R&D Systems	Cat# 3718-FB
Cycloheximide	Sigma-Aldrich	Cat# 18079
Blasticidin	InvivoGen	Cat# ant-bl-05
Tepotinib	Selleckchem	Cat# S7067
AZD4547	Selleckchem	Cat# S2801
TRIzol Reagent	Thermo Fisher Scientific	Cat# 15596026
Critical commercial assays		
Nano-Glo Dual-Luciferase Reporter Assay System	Promega	Cat# N1610
CyQUANT Cell Proliferation Assay Kit	Thermo Fisher	Cat# C35011
Maxwell RSC Blood DNA Kit	Promega	Cat# AS1400
Maxwell RSC miRNA Kit	Promega	Cat# AS1460
Zero Blunt TOPO PCR Cloning Kit	Thermo Fisher	Cat# 450031
Deposited data		
AACR Project GENIE v17	AACR	https://www.aacr.org/professionals/research/aacr-project-genie/
TCGA fusion dataset	NCI GDC	https://portal.gdc.cancer.gov
Raw data and analysis scripts	This study	https://doi.org/10.5281/zenodo.21804107
Experimental models: Cell lines		
EKVX (H. sapiens)	NCI	RRID: CVCL_1195
HT-29 (H. sapiens)	ATCC	RRID: CVCL_0320
SW948 (H. sapiens)	ATCC	RRID: CVCL_0632
CAPAN-1 (H. sapiens)	ATCC	RRID: CVCL_0237
786-O (H. sapiens)	ATCC	RRID: CVCL_1051
COLO-679 (H. sapiens)	DSMZ	RRID: CVCL_1130
SK-MEL-2 (H. sapiens)	ATCC	RRID: CVCL_0069
A172 (H. sapiens)	ATCC	RRID: CVCL_0131
LN405 (H. sapiens)	DSMZ	RRID: CVCL_1379
JHUEM7 (H. sapiens)	Creative Bioarray	RRID: CVCL_4658
SW756 (H. sapiens)	ATCC	RRID: CVCL_1727
SNU245 (H. sapiens)	Korean Cell Line Bank	RRID: CVCL_5038
TOV112D (H. Sapiens)	ATCC	RRID: CVCL_3612
T47D (H. Sapiens)	NCI	RRID: CVCL_0553
U2OS (H. Sapiens)	ATCC	RRID: CVCL_0042
Oligonucleotides		
Primers for TaqMan assays, 5′RACE, and Sanger sequencing, see Table S13	This study	N/A
Recombinant DNA		
pNLuc-AK3-hPGK	Addgene	242357
pNLuc-CAPZA2-hPGK	Addgene	242358
pNLuc-ETV1-hPGK	Addgene	242359
pNLuc-ETV4-hPGK	Addgene	242360
pNLuc-FGFR1-hPGK	Addgene	242362
pNLuc-FGFR2-hPGK	Addgene	242363
pNLuc-HELZ-hPGK	Addgene	242364
pNLuc-JAK2-hPGK	Addgene	242365
pNLuc-KAT7-hPGK	Addgene	242366
pNLuc-KCND3-hPGK	Addgene	242367
pNLuc-Kozak-hPGK (no UTR control)	Addgene	242368

(*Continued on next page*)

Continued

REAGENT or RESOURCE	SOURCE	IDENTIFIER
pNLuc-MET-hPGK	Addgene	242369
pNLuc-MTFR1-hPGK	Addgene	242370
pNLuc-NSD3-hPGK	Addgene	242371
pNLuc-NTRK2-hPGK	Addgene	242372
pNLuc-NUCKS1-hPGK	Addgene	242373
pNLuc-PPP6R3-hPGK	Addgene	242374
pNLuc-PTPRZ1-hPGK	Addgene	242375
pNLuc-SIK3-hPGK	Addgene	242376
pNLuc-SLC28A3-hPGK	Addgene	242377
pNLuc-SLC45A3-hPGK	Addgene	242378
pNLuc-SRGAP3-hPGK	Addgene	242379
pNLuc-ST7-hPGK	Addgene	242380
pNLuc-TEC-hPGK	Addgene	242381
pNLuc-TTC39B-hPGK	Addgene	242383
pNLuc-ACTB-hPGK	Addgene	252058
pNLuc-PTN-hPGK	Addgene	252059
pNLuc-RAC1-hPGK	Addgene	252060
pNLuc-ST7_1-hPGK	Addgene	252061
pNLuc-ST7_5-hPGK	Addgene	252062
pNLuc-minP-control	Addgene	252063
pNLuc-minP-6xETV1BSwt	Addgene	252064
pNLuc-minP-6xETV1BSmt	Addgene	252065
mApple_control	Addgene	252066
NoUTR_MET_Control	Addgene	252067
wtUTR_MET	Addgene	252068
CAPZA2_MET	Addgene	252069
ST7_MET	Addgene	252070
wtUTR_FGFR1	Addgene	252071
TEC_FGFR1	Addgene	252072
wtUTR_ETV1	Addgene	252073
MTFR1_ETV1	Addgene	252074
Software and algorithms		
R v4.5.1	R Foundation	https://www.r-project.org
ViennaRNA RNAfold v2.7.2	Lorenz et al.[32]	https://www.tbi.univie.ac.at/RNA/
ImageJ	NIH	https://imagej.nih.gov/ij/
IncuCyte Analysis Software	Sartorius	https://www.sartorius.com

EXPERIMENTAL MODEL AND STUDY PARTICIPANT DETAILS

Human cancer cell lines used in this study are listed in the Key Resources Table. Cells were cultured under the conditions specified in Table S7. Cell identity was verified by short tandem repeat (STR) profiling; cultures were routinely tested negative for mycoplasma contamination, and all experiments were performed within 10 passages after thawing.

METHOD DETAILS

Computational analysis

Fusion calls were obtained from AACR Project GENIE (v17.0-public)[24] and analyzed using R. For independent support analyses, TCGA fusion calls were processed using the same junction position-classification logic and reference coordinates. For each oncogene analyzed, reference chromosome, transcription start site (TSS) and start codon (ATG) coordinates were defined from curated RefSeq annotations. Partner-derived 5′UTR annotations were assigned using the corresponding MANE Select/RefSeq reference

transcripts and were used as a standardized framework for comparative analyses. These annotations provide a standardized reference for the partner-derived 5′UTR sequence but do not establish that the corresponding donor promoter or annotated TSS is used by the fusion allele. Oncogene side junction positions were classified as before_TSS (junction < TSS), within_5′UTR (TSS ≤ junction < ATG), or after_ATG (junction ≥ ATG). For RNA-supported fusion calls, this classification describes the position of the reported transcript junction relative to the reference transcript and does not necessarily resolve the underlying genomic breakpoint or promoter architecture. Analyses were restricted to fusion calls with precisely annotated oncogene-side junction positions to enable consistent classification relative to the translation start site. Where available, DNA- and RNA-support annotations reported by the AACR Project GENIE consortium were retained for each fusion call. These annotations were used to distinguish DNA-supported structural rearrangements from RNA-supported or support-unspecified fusion calls. The corresponding evidence for each retained MET fusion call is provided in Table S4. Putative uORFs were called using a conservative operational definition: an upstream AUG was counted as a uORF only if it initiated an open reading frame that terminated at the first downstream in-frame stop codon (UAA/UAG/UGA) upstream of the annotated main start codon. Overlapping uORFs in the same frame were conservatively merged and counted as one. For *MET*, experimentally validated uORFs were cross-referenced with the recently published TransCODE catalog of translated ORFs.[28] RNA folding propensity was estimated using MFE computed by ViennaRNA RNAfold (v2.7.2).[32] For comparative analyses, MFE was normalized by 5′UTR length (−MFE/nt). A composite 5′UTR complexity score was computed as an unweighted sum of the z-scores for 5′UTR length, uORF count, GC content, and normalized RNA folding stability (−MFE/nt). Z-scores were calculated relative to the reference distribution of all 17,999 protein-coding and oncogene 5′UTRs included in the analysis. Analyses were conducted in R (v4.5.1). Package versions and software details are provided in session information files deposited at Zenodo (https://doi.org/10.5281/zenodo.21804107).

Cell culture and treatments

All cell lines were cultured under conditions specified in Table S7. Cell identity was authenticated by short tandem repeat profiling, and cultures were regularly tested and confirmed negative for mycoplasma contamination. All experiments were performed using cells within 10 passages after thawing. Where indicated, cells were stimulated with recombinant human hepatocyte growth factor (HGF; R&D Systems, 294-HGN/CF) or recombinant human fibroblast growth factor 2 (FGF2; R&D Systems, 3718-FB). Timepoints and concentrations used are detailed in the figure legends.

Generation of stable cell lines

Stable cell lines were generated by lentiviral transduction. U2OS cells were transduced with ETV1 or FGFR1 lentiviral expression vectors, and T47D cells were transduced with MET expression constructs. A pLenti-mApple vector was used as infection control in all experiments. Infections were performed at a multiplicity of infection (MOI) of 0.5. Following transduction, cells were selected with Blasticidin (20 μg/mL for U2OS and T47D). Individual clones were isolated and expanded. For each construct, a minimum of 4–5 independent clones were established and validated prior to downstream analyses. All plasmids and lentiviral vectors used in this study are listed in Table S11, including Addgene accession numbers.

Western blotting

Cell lysates were prepared using hot Laemmli buffer as previously described.[29] Protein lysates were resolved on SDS–PAGE and transferred to PVDF membranes. Antibodies used for western blotting are listed in Table S12. Uncropped western blot images are provided in Data S1.

Polysome profiling

Polysome profiling was performed as previously described with minor modifications.[68] Briefly, cells were treated with cycloheximide (100 μg/mL, 10 min) prior to harvesting and lysed in polysome lysis buffer containing cycloheximide and RNase inhibitors. Lysates were layered onto 10–50% sucrose gradients and centrifuged at 35,000 rpm for 2 h at 4°C in a SW41 rotor (Beckman Coulter). Gradients were fractionated using an automated fractionation system with continuous monitoring at 254 nm. Fractions corresponding to light polysomes and heavy polysomes were defined based on A254 absorbance profiles. RNA was extracted from individual fractions using TRIzol and analyzed by RT–qPCR. TaqMan probes are listed in Table S13.

Cycloheximide chase assay

For protein stability assays, cells were treated with cycloheximide (100 μg/mL) and harvested at the indicated time points. Whole-cell lysates were analyzed by immunoblotting. Band intensities were quantified using ImageJ and normalized to loading controls. Protein decay curves were fitted using nonlinear regression (one-phase exponential decay), and half-lives were compared using linear mixed-effects modeling as described in the Statistical Analysis section.

Nucleic acid extraction and qPCR

Genomic DNA (gDNA) and total RNA were extracted using the Maxwell RSC Blood DNA Kit (Promega, AS1400) and the Maxwell RSC miRNA from Tissue and Plasma or Serum Kit (Promega, AS1460), respectively, according to the manufacturer's instructions. For copy number analysis, gDNA was analyzed using the TaqMan Copy Number Assay for *MET* (Table S13). For transcript quantification,

RNA was reverse-transcribed using SuperScript III Reverse Transcriptase (Invitrogen) with random hexamers, and RT-qPCR was performed using the TaqMan Gene Expression Assay for *MET* (Table S13) on a QuantStudio 5 system (Applied Biosystems). Data were analyzed using the ΔΔCt method, normalized to *TBP* (mRNA) or *hTERT* (gDNA) as internal controls.

Immunofluorescence

Cells were plated on glass coverslips. Fixation was performed in 4% paraformaldehyde for 10 min. After permeabilization (0.1% Triton X-100 in PBS with 0.2% BSA), samples were blocked in 3% BSA and incubated overnight at 4°C with primary antibodies (Table S12). Secondary antibodies were used at 1:400 for 1 h at room temperature (Table S12). Nuclei were counterstained with DAPI (1:3000) for 30 min before mounting. Images were acquired using identical acquisition settings across conditions.

Cell surface MET detection by flow cytometry

Cells (1×10^6 per well) were harvested, washed in PBS with 1% BSA, and incubated in 5% BSA for 30 min at 4°C to block non-specific binding. Cells were stained with a PE-conjugated anti-MET antibody (Table S12) for 30 min on ice. After three washes in PBS with 1% BSA, cells were resuspended in PBS and analyzed on a ThermoFisher Attune NxT flow cytometer. At least 20,000 events were collected per sample. Gating strategies are provided in Data S2.

NanoLuc reporter assay

Cells were transfected with NanoLuc-encoding reporter constructs containing the indicated 5′UTRs upstream of the same coding sequence under the control of the *hPGK* promoter. Plasmids used are detailed in Table S11. Luminescence was measured 24 h post-transfection using the Nano-Glo Dual-Luciferase Reporter Assay System (Promega, N1610) according to the manufacturer's protocol. Firefly luciferase-expressing pGL4.53 vector (Promega, E5011) served as a normalization control.

Irradiation and survival assays

Cells were irradiated with 7.5 Gy using a CellRad precision X-ray irradiator (Precision X-ray, North Branford, CT) at room temperature. For short-term survival, viability was measured 48 h post-irradiation using the CyQUANT Cell Proliferation Assay Kit (ThermoFisher, C35011), following the manufacturer's instructions. For long-term survival, irradiated cells were seeded at low density and cultured for 10–14 days. Colonies were fixed and stained with 0.5% crystal violet in 25% methanol, and the stain was solubilized in 10% acetic acid. Absorbance was measured at 590 nm to quantify the relative colony-forming capacity.

Wound healing assay

Scratch assays were performed using the IncuCyte WoundMaker tool (Sartorius). Confluent monolayers were scratched, and wound closure was monitored for the indicated duration using the IncuCyte Live-Cell Analysis System. Wound confluence was quantified using IncuCyte software.

5′ rapid amplification of cDNA ends (5′RACE)

5′RACE was performed using a modified SMARTer-based protocol. Reverse transcription was carried out using SuperScript IV Reverse Transcriptase (Thermo Fisher, 18090050) and a MET gene-specific primer (GSP1), in combination with a template-switching oligo (TSO). The resulting cDNA contained a 5′ universal adapter sequence. First-round PCR was performed using Q5 Hot Start DNA Polymerase (NEB) with a forward primer complementary to the TSO adapter and a nested MET reverse primer (GSP2), located upstream of GSP1. All primer sequences are listed in Table S13. Amplification products were purified and cloned into the Zero Blunt TOPO PCR Cloning Kit (Thermo Fisher, 450031) and transformed into NEB high-efficiency competent cells. Positive colonies were screened by PCR using M13R and T7 primers and confirmed by Sanger sequencing (N = 48 clones per condition across two independent 5′RACE experiments). Only sequences with unambiguous chromatograms and clear junction mapping were retained for analysis. Sequencing raw data are available at Zenodo (https://doi.org/10.5281/zenodo.21804107).

QUANTIFICATION AND STATISTICAL ANALYSIS

Statistical analyses were performed using R (v4.5.1). Statistical tests, sample sizes (n), measures of central tendency, dispersion, and exact p values are indicated in the corresponding figure legends. Unless otherwise stated, data are presented as mean ± SEM. Statistical significance was defined as $p < 0.05$. Nonlinear regression and linear mixed-effects models were used as described in the relevant method details sections. No statistical methods were used to predetermine sample size. Experiments were independently repeated as indicated in the figure legends.

Additional resources

Source code, session information files, and raw sequencing data are available through the Zenodo repository (https://doi.org/10.5281/zenodo.21804107).

Cell Reports, Volume *45*

Supplemental information

Untranslated region rewiring defines a novel class of oncogene fusions

Marina Cerqua, Estelle Bigot, Cédric Chaveroux, Paolo M. Comoglio, and Dogus M. Altintas

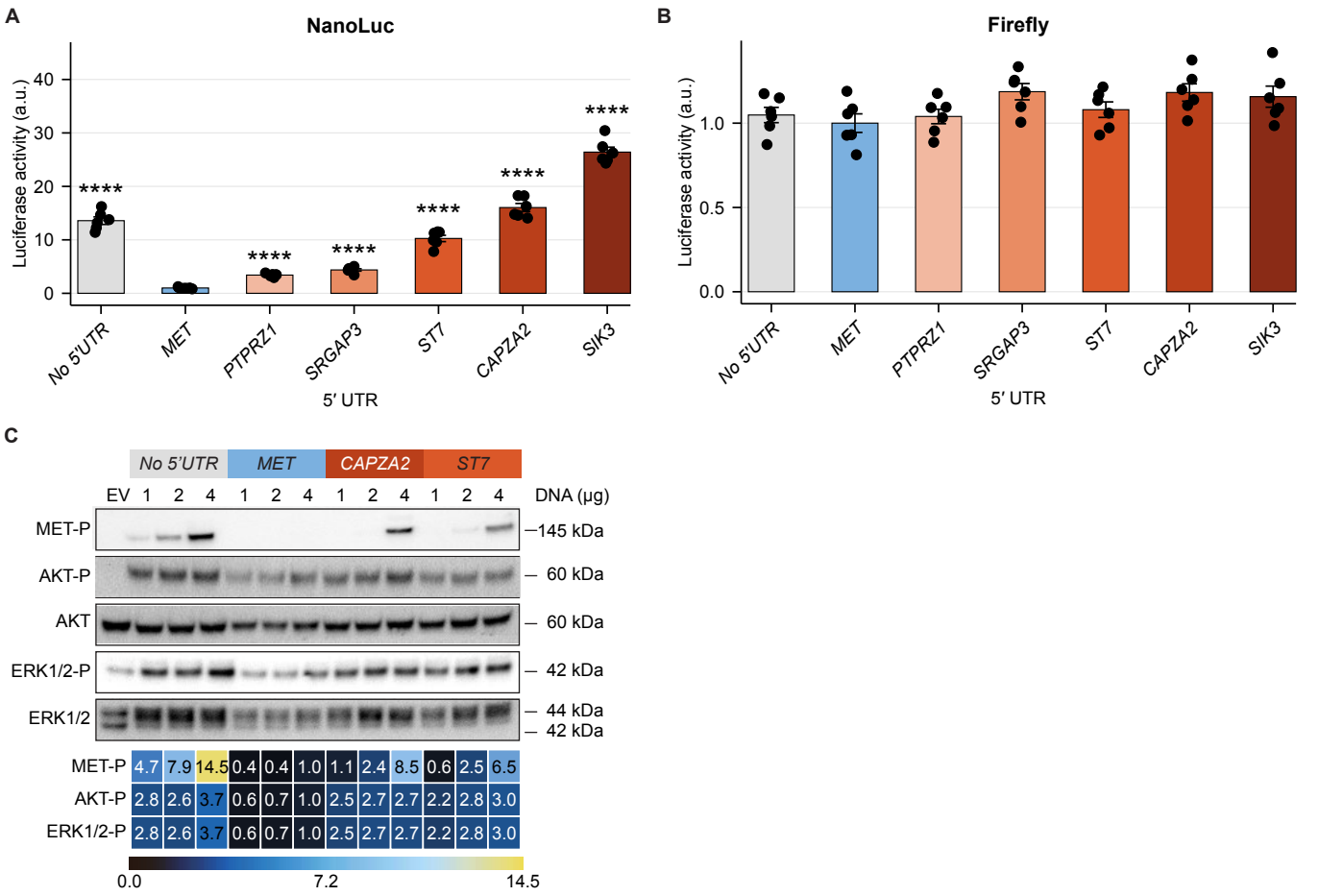


Figure S1. Donor-derived 5′UTRs enhance translational output and MET signalling.

(A) NanoLuc luminescence values prior to NanoLuc/Firefly normalisation corresponding to Figure 2A. Each dot represents one independent biological replicate (n = 6 independent biological replicates). Statistical analysis was performed using one-way ANOVA followed by Dunnett's post hoc test versus the native *MET* 5′UTR.
(B) Firefly luciferase activity measured from the same transfections as in panel A. Firefly luminescence values are shown to confirm comparable transfection efficiency across constructs. Data represent mean ± s.e.m. (n = 6 independent biological replicates). No significant differences were observed between groups (ANOVA followed by Dunnett's multiple-comparisons test versus the native *MET* 5′UTR).
(C) TOV112D cells were transfected with *MET* expression vectors containing either no 5′UTR, the native *MET* 5′ UTR, or donor-derived 5′UTRs (*CAPZA2* or *ST7*). Immunoblots show p-MET and transducers (p-AKT and p-ERK1/2) following 15 min HGF (20 ng/mL) stimulation. Blots are representative of n = 3 independent biological experiments.



Figure S2. Sanger sequencing confirms preservation of the *MET* coding sequence in fusion-positive cell lines.

Alignment of the *MET* coding sequence obtained by Sanger sequencing from fusion-positive cell lines used in this study (JHUEM7, SNU245, SW756) compared with the reference MET protein sequence derived from the fusion-negative A172 or LN405 cell lines. Amino acid alignment demonstrates complete preservation of the MET protein sequence in all fusion-positive models, with no additional missense, nonsense, or frameshift variants detected.

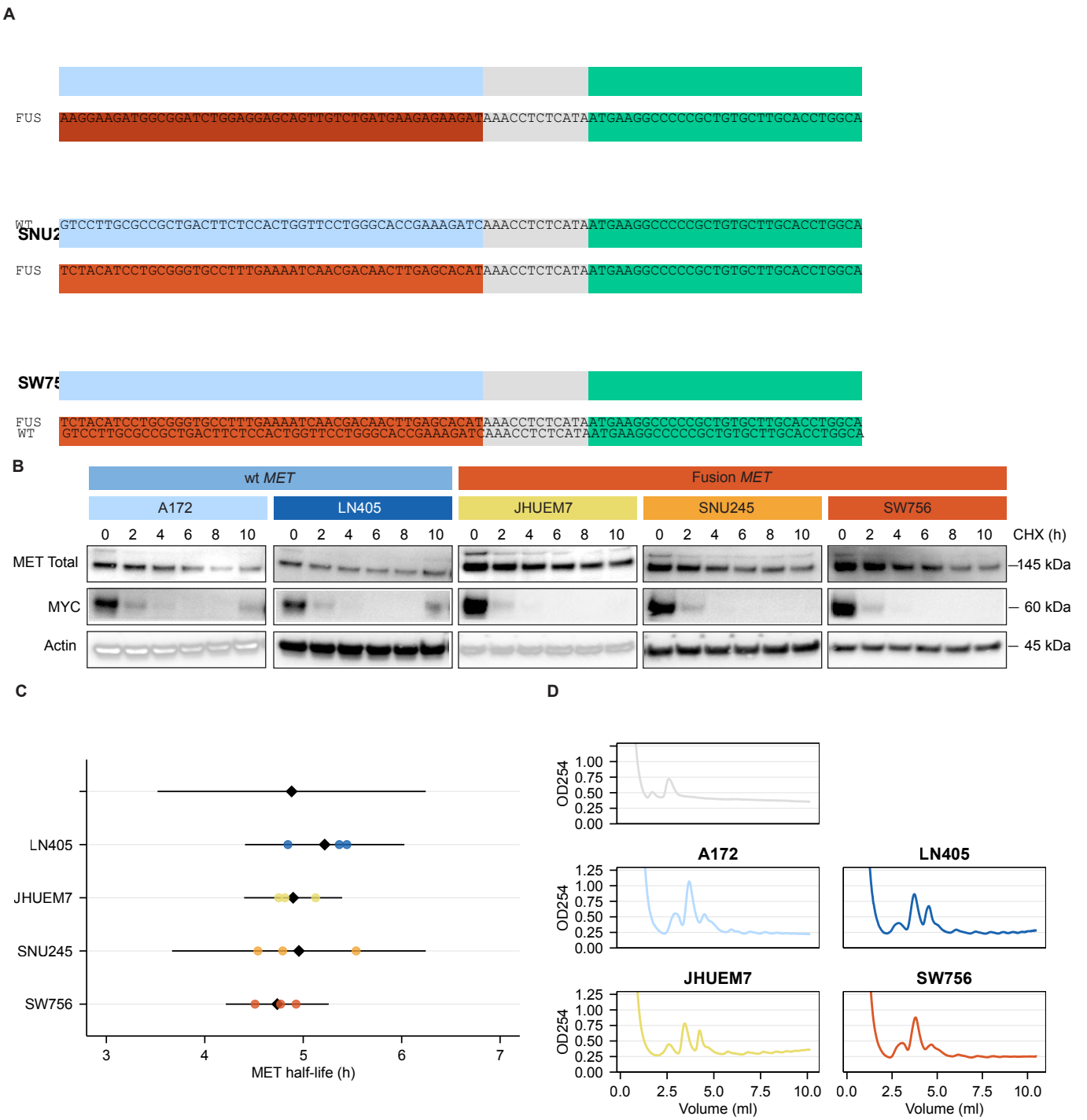


Figure S3. Translational basis of MET upregulation.

(A) Sanger sequencing of 5′RACE products from fusion-positive cell lines compared with wild-type reference sequences to characterise 5′UTR architecture. Colour coding indicates sequence origin: blue, native *MET* 5′ UTR; grey, retained 5′UTR segments; red, donor-derived fusion 5′UTRs; green, *MET* CDS. All validated fusion events replace the native *MET* 5′UTR upstream of the canonical start codon (ATG).
(B) Representative western blots from cycloheximide (CHX) chase experiments assessing MET protein stability in fusion-positive and wild-type models. Cells were treated with CHX and harvested at the indicated time points. Immunoblots show total MET and actin loading control. c-Myc was included as a short-lived protein control to verify effective translation inhibition. Blots are representative of n = 3 independent biological experiments.
(C) Quantification of CHX chase experiments shown in panel B. MET protein levels were normalised to actin and expressed relative to time zero. Data represent mean ± s.e.m. from n = 3 independent biological replicates. Statistical analysis was performed on estimated half-lives (t½) using a linear mixed-effects model (t½ ~ genotype + (1|cell line)); genotype differences were assessed using an emmeans contrast (WT − Fusion). No significant differences in MET decay kinetics were observed between fusion-positive and wild-type models, indicating that altered protein stability does not explain MET upregulation.
(D) Representative A254 absorbance traces from polysome profiling analyses of fusion-positive and wild-type models. The traces represent n = 3 independent biological replicates.

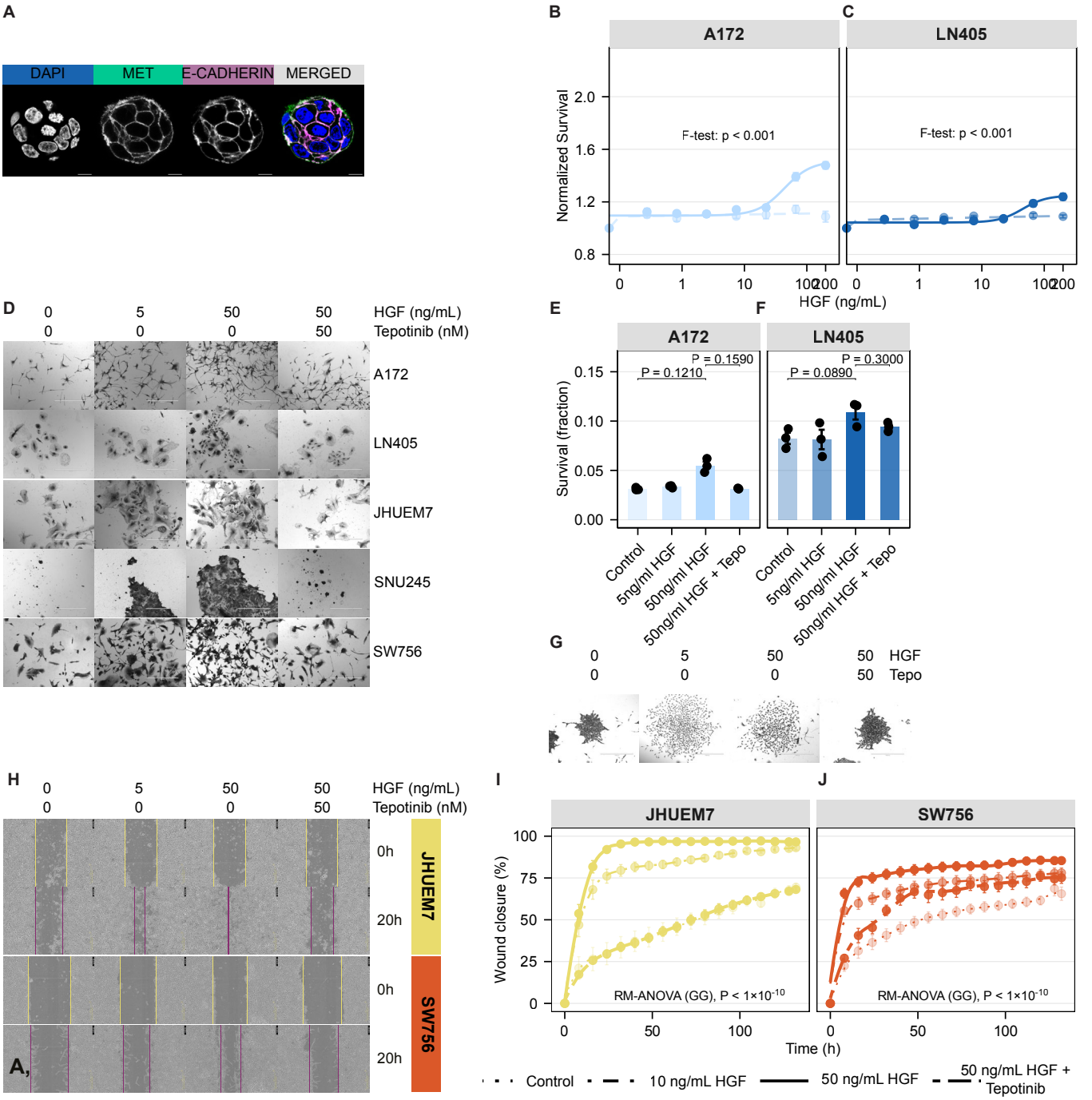

A
DAPI
MET
E-CADHERIN
MERGED
B
C
A172
LN405
Normalized Survival
F-test: p < 0.001
F-test: p < 0.001
HGF (ng/mL)
D
HGF (ng/mL)
Tepotinib (nM)
A172
LN405
JHUEM7
SNU245
SW756
E
F
A172
LN405
Survival (fraction)
P = 0.1210
P = 0.1590
P = 0.0890
P = 0.3000
Control
5ng/ml HGF
50ng/ml HGF
50ng/ml HGF + Tepo
G
HGF
Tepo
H
HGF (ng/mL)
Tepotinib (nM)
0h
20h
JHUEM7
SW756
I
J
JHUEM7
SW756
Wound closure (%)
RM-ANOVA (GG), P < 1×10-10
Time (h)
Control
10 ng/mL HGF
50 ng/mL HGF
50 ng/mL HGF + Tepotinib

Figure S4. Functional validation of HGF responsiveness.

(A) Immunofluorescence staining of SNU245 cells showing MET (green) and E-cadherin (magenta) with DAPI (blue). Representative images of n = 3 independent experiments. Scale bar, 25 μm.
(B-C) Dose–response curves of normalised survival in A172 (B) and LN405 (C) cells following increasing HGF concentrations, in the presence or absence of Tepotinib (50 nM). Data represent mean ± s.e.m. (n = 3 independent biological replicates). Statistical significance determined by nonlinear regression comparison using the extra sum-of-squares F-test.
(D) Representative images of clonogenic assays performed in the indicated cell lines 14 days after treatment with indicated HGF concentrations ± Tepotinib. Colonies were fixed and stained with crystal violet. Images are representative of n = 3 independent biological experiments.
(E-F) Quantification of clonogenic growth in A172 (E) and LN405 (F) cells under the indicated conditions. Colony formation was quantified by crystal violet absorbance. Bars represent mean ± s.e.m. (n = 3 independent biological experiments). Statistical significance was assessed using one-way ANOVA followed by Tukey's multiple-comparisons test.
(G) Representative scattering response to indicated concentrations of HGF ± Tepotinib (50 nM) in SW756 cells.
(H) Representative wound healing images at 0 h and 20 h following HGF stimulation ± Tepotinib in JHUEM7 and SW756 cells (n = 6 independent biological experiments).
(I-J), Quantification of wound closure over time in JHUEM7 (I) and SW756 (J) cells. Data represent mean ± s.e.m. (n = 6 independent biological experiments). Statistical significance was assessed using repeated-measures ANOVA with Greenhouse–Geisser correction.

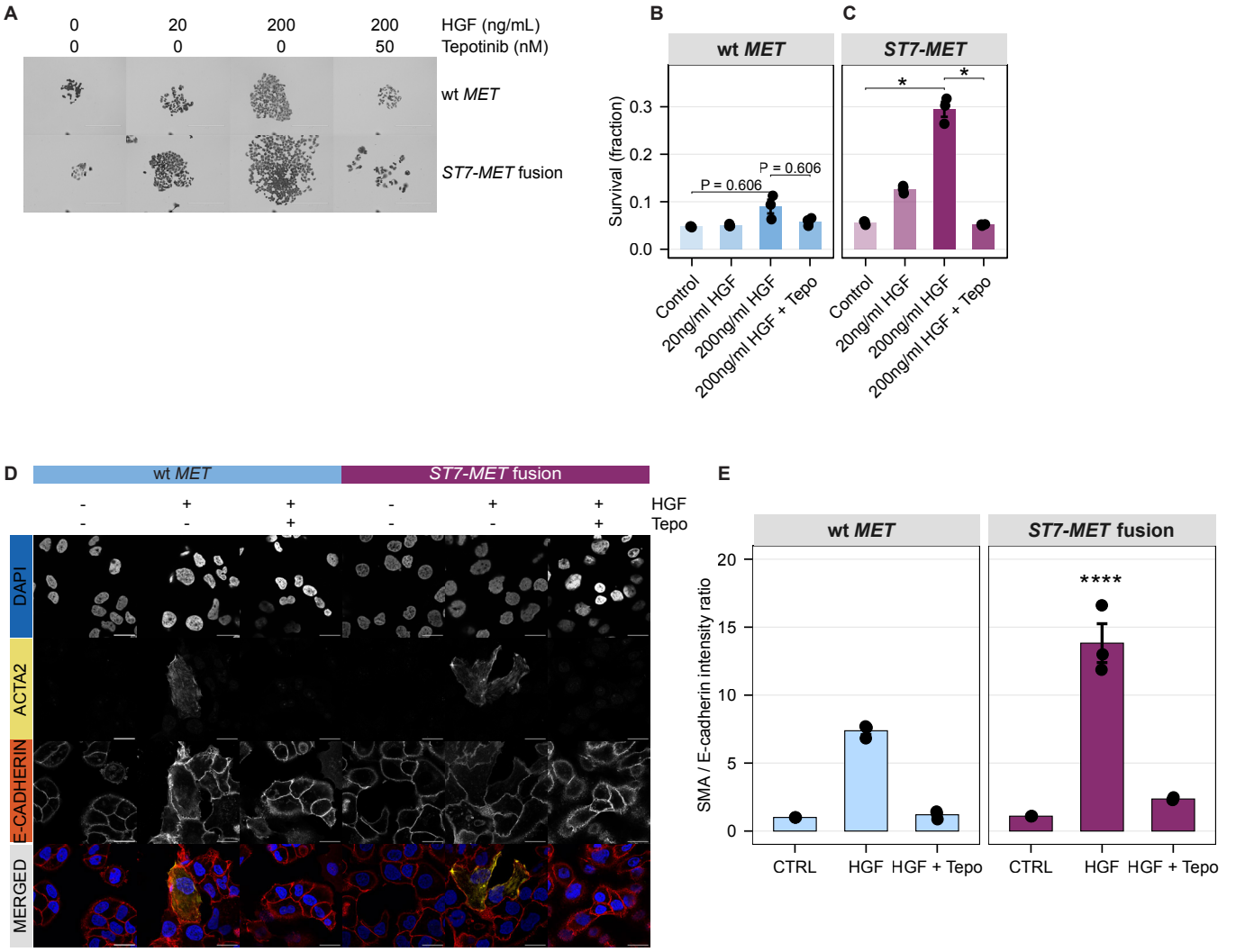
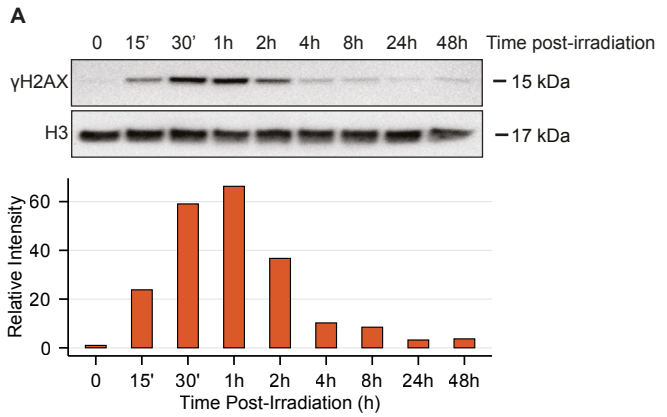
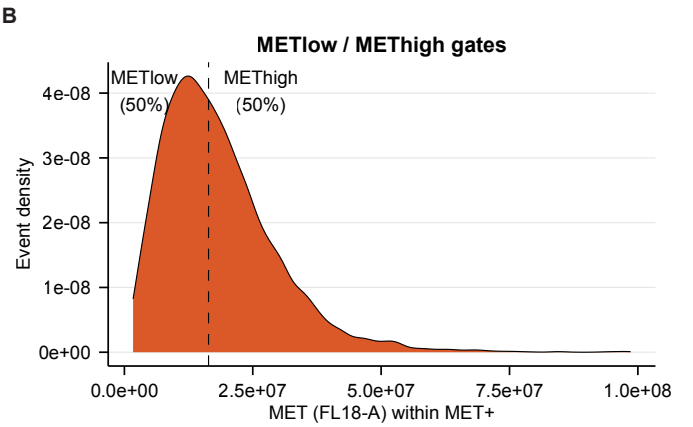
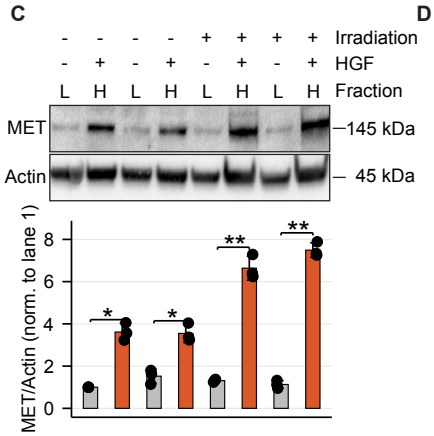


Figure S5. Functional characterisation of T47D cells expressing wild-type or *ST7–MET* 5′UTR constructs.

(A) Representative brightfield images of T47D cells expressing wt *MET* or *ST7–MET* fusion, treated with indicated concentrations of HGF in the presence or absence of Tepotinib (50 nM). Images were acquired 10–14 days post-irradiation following clonogenic recovery. Images are representative of n = 3 independent biological experiments.
(B–C) Quantification of clonogenic survival in T47D cells expression wild-type (B) or *ST7-MET* fusion (C) under the indicated conditions. Survival fraction was determined by crystal violet staining followed by absorbance measurement. Bars represent mean ± s.e.m. (n = 3 independent biological replicates). Statistical analysis was performed using one-way ANOVA followed by Tukey's multiple-comparisons test.
(D) Representative immunofluorescence images of EMT markers in T47D cells expressing either wt *MET* or *ST7-MET* fusion treated with HGF ± Tepotinib (50 nM). Cells were stained for E-cadherin and ACTA2 (α-SMA); nuclei were counterstained with DAPI. Images are representative of n = 3 independent biological experiments. Scale bar, 25 µm.
(E) Quantification of EMT marker expression in T47D wild-type and *ST7-MET* fusion cells. The ACTA2/E-cadherin fluorescence intensity ratio was calculated at the single-cell level. Data represent mean ± s.e.m. from n = 3 independent biological experiments. Statistical analysis was performed using a linear model followed by estimated marginal means (emmeans) contrasts with Tukey adjustment (****P<0.0001; comparison between wt *MET* and *ST7-MET* in the presence of HGF).



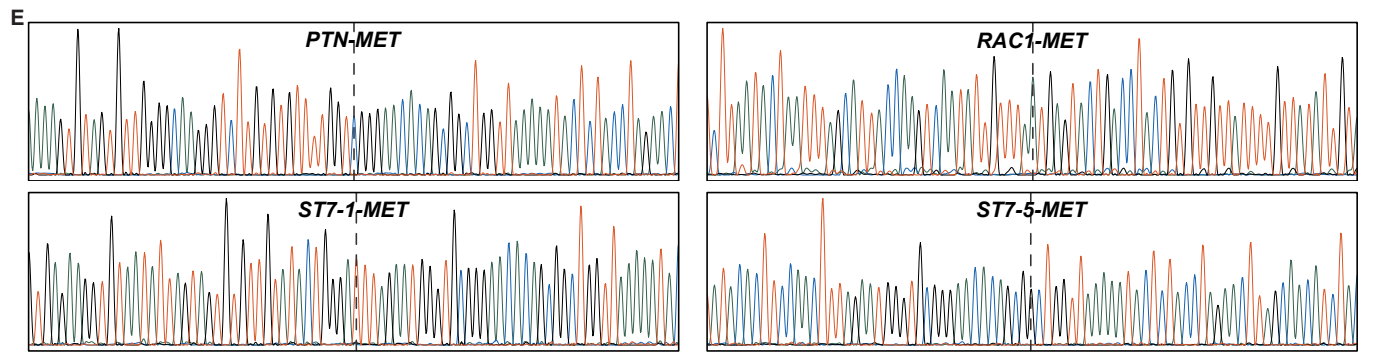


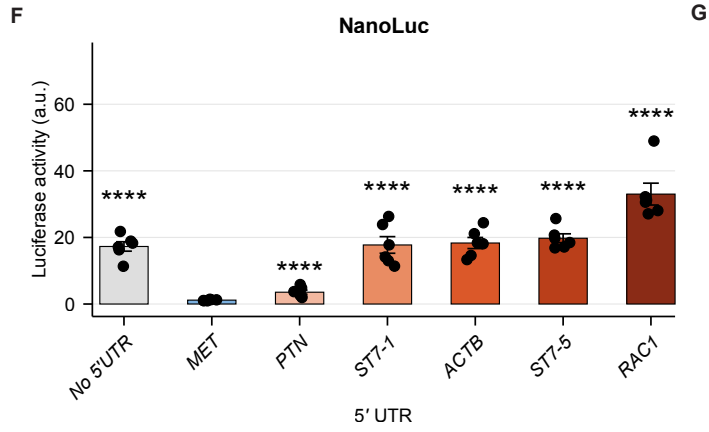


D

Features of MET 5′ UTR and fusion-derived 5′ UTRs

5′ UTR Architecture	5′ UTR Length (nt)	# uORFs	GC Content (%)	MFE (kcal/mol)	Complexity score
MET	**396**	**2**	**75**	**-225.8**	**3.98**
PTN	220	0	57	-57.7	-1.02
ST7-1	66	0	56	-12.7	-2.85
ACTB	98	0	69	-14.4	-1.17
ST7-5	70	0	57	-17.8	-2.29
RAC1	182	0	63	-69.4	0.22





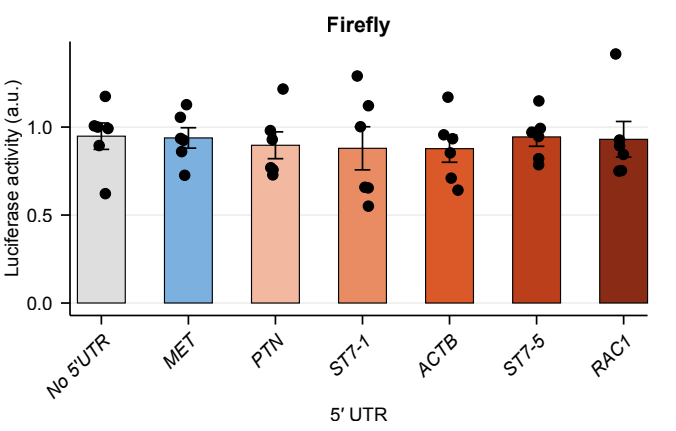
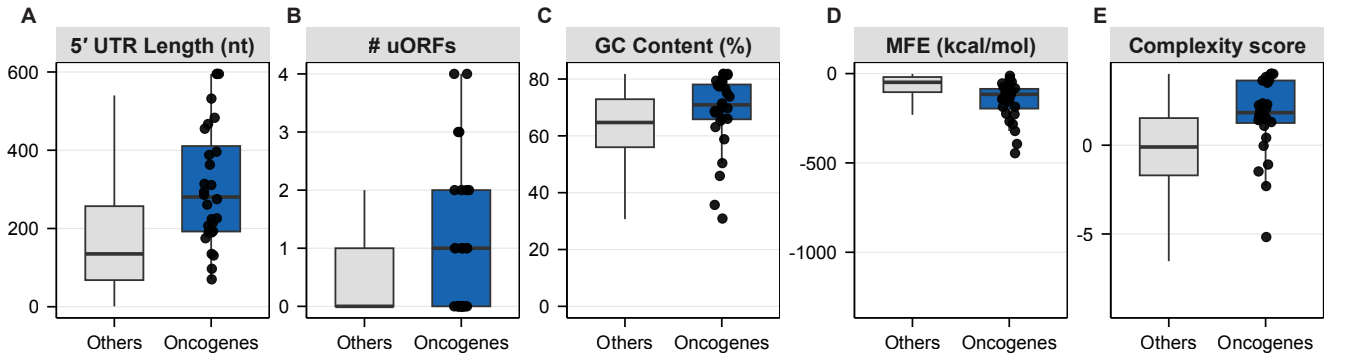


Figure S6. Validation of irradiation response, MET sorting, and fusion transcript characterization.

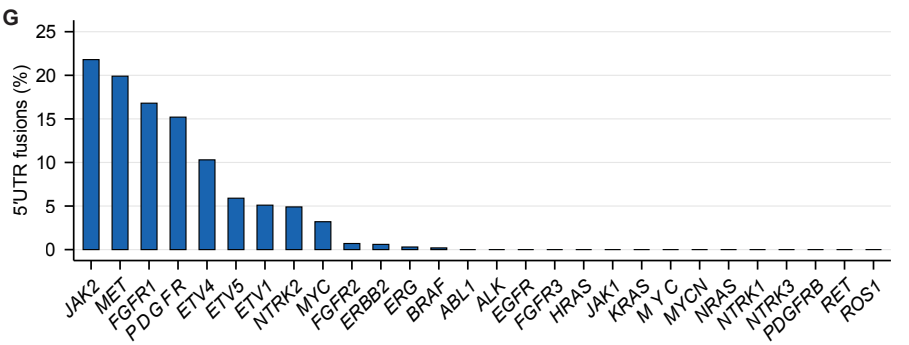
(A) Immunoblot analysis of the DNA damage marker γH2AX following 7.5 Gy irradiation in A172 cells. γH2AX signal increases within the first hours and declines thereafter. Quantification of γH2AX intensity, normalized to the H3 loading control, is shown below.
(B) Representative flow cytometry profile showing separation of MET^{low} and MET^{high} populations based on surface MET expression in non-irradiated control cells. Data are representative of n = 3 independent experiments.
(C) Immunoblot validation of sorted MET^{low} (L) and MET^{high} (H) populations under the indicated irradiation and HGF conditions. MET protein levels are higher in MET^{high} fractions relative to MET^{low} fractions. Quantification is shown below. Data represent mean ± SEM from n = 3 independent biological replicates. Statistical significance was assessed using two-tailed paired t-tests with Benjamini–Hochberg correction.
(D) Features of the native MET 5′UTR and donor-derived 5′UTRs, including length, uORF number, GC content, minimum free energy (MFE), and complexity score.
(E) Representative Sanger chromatograms of identified 5′UTR-replacing fusion transcripts (*PTN–MET*, *ST7-1–MET*, *ST7-5–MET*, *RAC1–MET*). Vertical dashed lines indicate fusion junctions. Junctions were validated by forward and reverse sequencing. All raw sequencing files are available at Zenodo (https://doi.org/10.5281/zenodo.21804107).
(F) NanoLuc reporter activity. Data represent mean ± SEM from n = 6 independent biological replicates. Statistics: one-way ANOVA with Dunnett's post-hoc test vs MET 5'UTR (****P<0.0001).
(G) Firefly control reporter activity demonstrating comparable transfection efficiency across constructs. Data represent mean ± SEM from n = 6 independent biological replicates.



F

5′ UTR features: oncogenes versus protein-coding genes.

Metric	Protein-coding genes (median [IQR])	Oncogenes (median [IQR])	Wilcoxon p
5′ UTR Length (nt)	135.00 [189.00]	280.50 [218.50]	8.97e-06
# uORFs	0 [1]	1 [2]	0.052
GC Content (%)	64.7 [16.9]	70.9 [12.2]	0.00664
MFE (kcal/mol)	-48.80 [84.65]	-116.10 [110.47]	2.81e-06
Complexity score	-0.10 [3.23]	1.83 [2.39]	1.7e-05



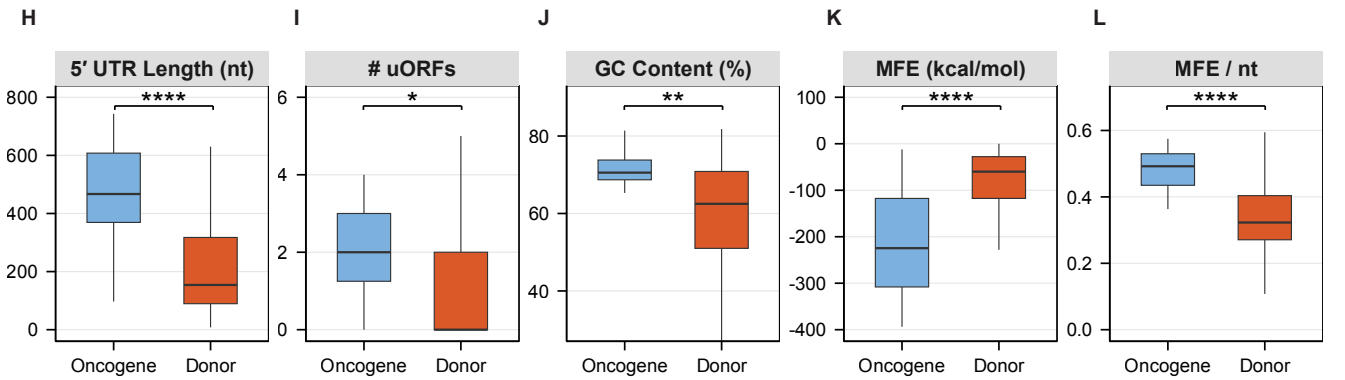


Figure S7. Oncogenes harbor complex 5′UTRs compared with the human transcriptome and are preferentially rewired by simpler donor 5′UTRs.

(A–E) Distribution of individual 5′UTR features across the human transcriptome, comparing the 27 oncogenes analyzed to all other protein-coding genes: 5′UTR length (A), number of upstream open reading frames (uORFs) (B), GC content (C), minimum free energy (MFE) (D), and the composite 5′UTR complexity score (E). Boxes indicate median and interquartile range (IQR); points represent individual genes.
(F) Summary statistics for the features shown in panels A–E. The table reports median [IQR] values for protein-coding genes versus oncogenes, along with two-sided Wilcoxon rank-sum test P-values for each feature.
(G) Frequency of untranslated-region rewiring across oncogenes harboring 5′UTR-replacing fusions. Bars show, for each oncogene, the percentage of 5′UTR-replacing (“untranslated region rewiring”) fusions among all fusions involving that oncogene.
(H–L) Pairwise comparisons between oncogenes and their donor (fusion partner) genes in 5′UTR-replacing fusions: 5′UTR length (H), uORF count (I), GC content (J), MFE (K), and normalised folding stability (MFE/nt) (L). Statistical significance was assessed using a two-sided paired Wilcoxon signed-rank test across oncogene–donor pairs. ****P < 0.0001; **P < 0.01; *P < 0.05.

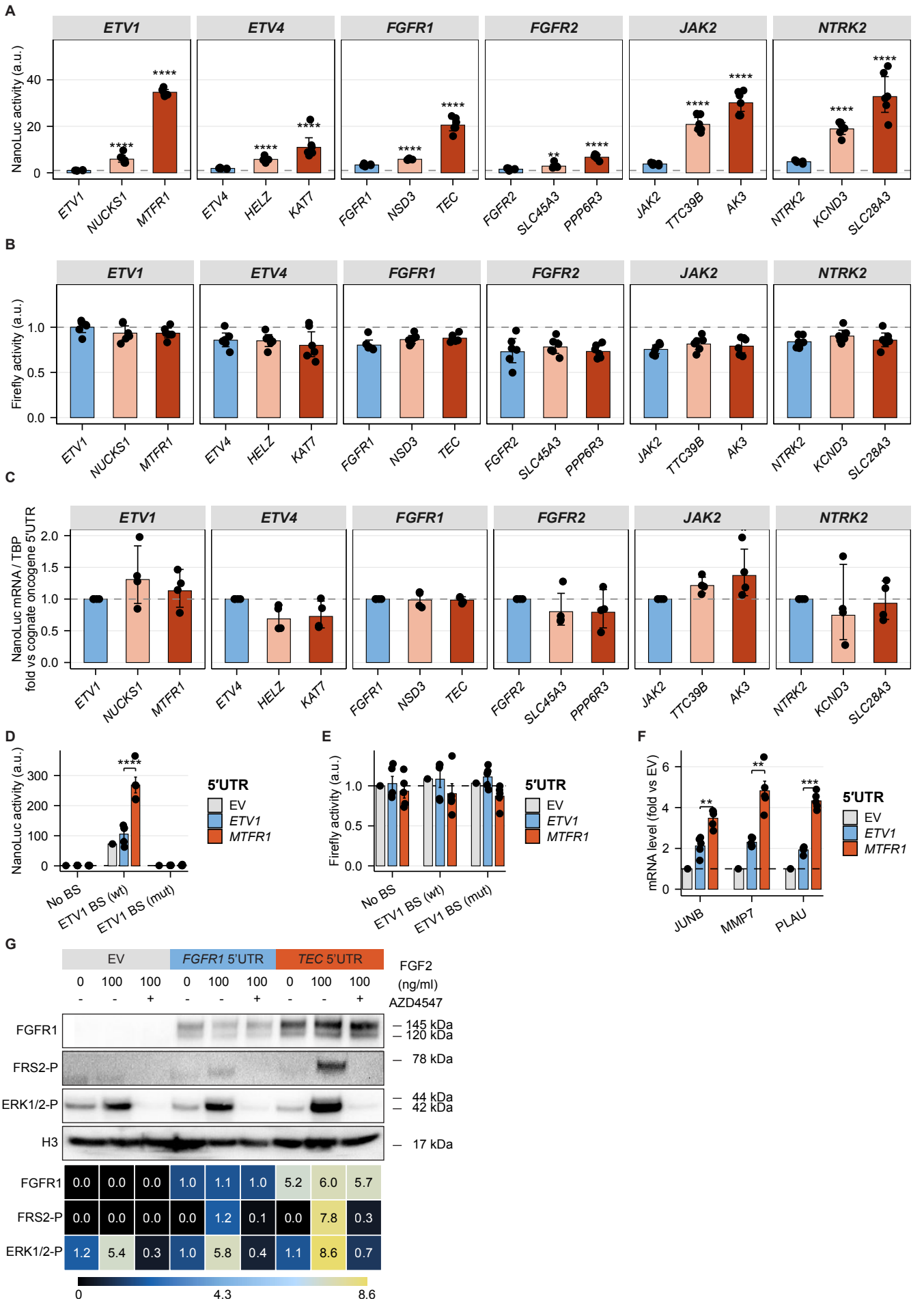

A
ETV1
ETV4
FGFR1
FGFR2
JAK2
NTRK2
NanoLuc activity (a.u.)
ETV1 NUCKS1 MTFR1
ETV4 HELZ KAT7
FGFR1 NSD3 TEC
FGFR2 SLC45A3 PPP6R3
JAK2 TTC39B AK3
NTRK2 KCND3 SLC28A3
B
Firefly activity (a.u.)
C
NanoLuc mRNA / TBP
fold vs cognate oncogene 5'UTR
D
NanoLuc activity (a.u.)
No BS
ETV1 BS (wt)
ETV1 BS (mut)
5'UTR
EV
ETV1
MTFR1
E
Firefly activity (a.u.)
F
mRNA level (fold vs EV)
JUNB
MMP7
PLAU
G
EV
FGFR1 5'UTR
TEC 5'UTR
FGF2
(ng/ml)
AZD4547
FGFR1
FRS2-P
ERK1/2-P
H3
145 kDa
120 kDa
78 kDa
44 kDa
42 kDa
17 kDa
0.0 0.0 0.0 1.0 1.1 1.0 5.2 6.0 5.7
0.0 0.0 0.0 0.0 1.2 0.1 0.0 7.8 0.3
1.2 5.4 0.3 1.0 5.8 0.4 1.1 8.6 0.7
0
4.3
8.6

Figure S8. 5′UTR fusions generalize to oncogenes with complex untranslated regions.

(A) NanoLuc reporter activity values corresponding to the oncogene and donor 5′UTR constructs shown in Figure 6B, shown without ratio normalization. Bars show mean ± SEM (n = 6 independent biological replicates) Statistical testing was performed as in Figure 6B (one-way ANOVA with Dunnett's post hoc test versus the native oncogene 5′UTR).
(B) Firefly luciferase activity measured from the same transfections as in panel A, shown without ratio normalization to confirm comparable transfection efficiency across constructs (mean ± SEM, n = 6).
(C) Relative NanoLuc mRNA levels measured by RT–qPCR from the same transfections, normalized to Firefly mRNA and expressed relative to the native oncogene 5′UTR (mean ± SEM, n = 6).
(D) NanoLuc reporter activity from the ETV1 binding-site experiment (pNLuc_minP_ETV1BS), comparing reporters containing no binding site (No_BS), a wild-type ETV1 binding site (ETV1 BS (wt)), or a mutated binding site (ETV1 BS (mut)), in cells expressing ETV1 under the control of either the native *ETV1* 5′UTR or the *MTFR1* donor-derived 5′UTR. Data are shown as mean ± SEM with individual biological replicates (n = 5 independent clones). Data were analysed using a linear model including a UTR × construct interaction term, followed by emmeans contrasts with Holm correction (****P < 0.0001).
(E) Firefly luciferase activity from the same ETV1 binding-site experiment shown in panel D, shown without ratio normalisation (mean ± SEM n = 5 independent clones).
(F) RT–qPCR analysis of ETV1 target gene expression in cells stably integrated with an empty vector control (EV), *ETV1* with the native 5′UTR, or *ETV1* with the MTFR1 donor-derived 5′UTR. Expression levels are shown relative to EV (mean ± SEM; n = 3 biological replicates).
(G) Western blot analysis of FGFR1 signalling in cells stably integrated with EV, native FGFR1 5′UTR, or the donor-derived TEC 5′UTR (TEC–FGFR1) constructs. Cells were treated with ± FGF2 (100 ng/mL) ± the FGFR inhibitor AZD4547 (500 nM) for 15 minutes. Immunoblots show FGFR1, p-FRS2, p-ERK1/2, and H3 as a loading control.